C.V

NACA

RESEARCH MEMORANDUM

ANALYSIS OF TURBOMACHINE VISCOUS LOSSES AFFECTED BY CHANGES IN BLADE GEOMETRY

By James W. Miser, Warner L. Stewart, and Warren J. Whitney

Lewis Flight Propulsion Laboratory
Cleveland, Ohio

NATIONAL ADVISORY COMMITTEE
FOR AERONAUTICS

WASHINGTON

October 2, 1956

NACA RM E56F21

NATIONAL ADVISORY COMMITTEE FOR AERONAUTICS

RESEARCH MEMORANDUM

ANALYSIS OF TURBOMACHINE VISCOUS LOSSES AFFECTED BY CHANGES IN BLADE GEOMETRY

By James W. Miser, Warner L. Stewart, and Warren J. Whitney

SUMMARY

The effect of changes in blade geometry on the viscous losses in turbomachines is analyzed. The variables affected by changes in blade geometry that are considered are blade number, solidity, aspect ratio, Reynolds number, and trailing-edge blockage. For changes in blade geometry that involve a change in blade chord length, the viscous losses are assumed to vary inversely as the one-fifth power of the flow Reynolds number based on the blade chord length.

Viscous loss can be expressed as a function of three variables: the blade height-to-spacing ratio, the solidity, and a height Reynolds number. Variations of the first two result in counteracting effects of the endwall or the blade surface areas, or both, and the momentum loss per unit surface area. Thus, optimum values of blade number and solidity can be determined for the example turbine experimental data presented. However, for variations in the height Reynolds number, there is no effect of area to counteract the effect of changes in the chord Reynolds number; therefore, for every increase in the height Reynolds number an improvement in aerodynamic performance is predicted.

In the analysis it is determined that the blade number can be changed over a wide range from the optimum value with little effect on blade viscous loss. For changes of solidity only, experimental data indicate that solidity can be varied over a more limited range with very little effect on the blade viscous loss.

Because changes in the trailing-edge blockage also affect the blade total-pressure loss, the effect of varying trailing-edge blockage is analyzed. Trailing-edge blockage might affect to a large extent the number of blades that correspond to the minimum total-pressure loss, especially for large trailing-edge thicknesses.

INTRODUCTION

As part of the NACA turbomachine research program, the various factors that affect the source and magnitude of the aerodynamic losses within blade rows are being studied. The results of these investigations should provide the basis for design of more efficient turbines and point to new areas of research.

The principal aerodynamic losses in turbomachines are attributed to the development of a boundary layer on the surfaces of the blades and the inner and outer walls. Recent investigations have been made with regard to the possibility of correlating losses in turbomachines on the basis of basic boundary-layer parameters. Reference 1 describes the basic boundary-layer parameters at the blade trailing edge and presents a method for calculating a two-dimensional loss from these parameters for an assumed simple-power-law velocity profile. Reference 2 shows that blade wakes obtained experimentally can be satisfactorily approximated by the simple-power-law velocity profile with an exponent of 1/7. Reference 3 presents a means of obtaining a three-dimensional loss based on mean-section boundary-layer parameters that are assumed to represent the average momentum loss over both the blade and the end walls. On the basis of the preceding investigations, reference 4 presents a method of obtaining an effective momentum thickness for rotors based on turbine over-all performance and knowledge of stator losses.

Using the relations between boundary-layer parameters and blade loss developed in references 1 to 4, an analysis is made herein of the effect of changes in blade geometry on the viscous losses in turbomachines. The variables affected by changes in blade geometry that are considered are blade number, solidity, aspect ratio, and Reynolds number.

This report also presents a method of optimizing the blade number and solidity for a given application if the blade loss variation with solidity can be estimated or experimentally determined. Also discussed are the penalties in performance that accompany deviations from optimum values of blade number and solidity. Because trailing-edge blockage affects the selection of blade number, its effect on blade losses is also considered.

METHOD OF ANALYSIS

The over-all blade losses considered in this report can be divided into two parts: (1) the blade viscous loss resulting from the development of a boundary layer on the blade surface and (2) the mixing loss associated with the mass-flow void behind the blade trailing edge. For a given trailing-edge blockage and flow velocity diagram, the blade viscous loss can be considered to be independent of that due to the

trailing-edge blockage. However, in determining the optimum number of blades on the basis of the minimum over-all blade loss, the effect of the trailing-edge blockage must be considered. For this reason, the effect of trailing-edge blockage on over-all blade loss is discussed in the section entitled RESULTS OF ANALYSIS.

If the blade viscous loss is considered to be independent of the effect of trailing-edge blockage, a relation between blade geometry and blade viscous loss can be developed. From this relation, optimum values of some of the blade geometric quantities are obtained, and then the effects of deviating from these optimum values are determined.

In reference 1, changes in the over-all blade viscous loss were found to be directly related to the momentum thickness at the trailing edge expressed in terms of a momentum-thickness parameter θ^*. (See appendix A for definitions of symbols used in this report.) Therefore, changes in the value of the momentum-thickness parameter θ^* are used herein to represent the trends of changes in the blade viscous loss with changes in the blade geometry.

Throughout this report, fully developed turbulent-boundary-layer conditions are assumed. For turbomachines, this assumption appears to be in good agreement with experimental results (see ref. 2).

Relation between Blade Geometry and Blade Viscous Loss

As a fluid passes over any surface, a boundary layer develops because of the viscosity of the fluid. The viscous loss resulting from the development of the boundary layer is often described in terms of a momentum thickness θ (see ref. 1). Considering the two-dimensional blade shown in figure 1, a boundary layer would build up on both the suction and pressure surfaces; therefore, there would be a momentum thickness for each surface, namely θ_s and θ_p. The sum of the momentum thickness on each surface is termed a total momentum thickness θ_{tot}.

In reference 4, the average blade surface length was closely approximated by the blade mean camber length. This reference also pointed out that the ratio of the blade mean camber length to the blade chord length c is almost a constant for a given velocity diagram over a wide range of solidities. In the subsequent development, it is more advantageous to express the two-dimensional blade surface area in terms of the blade chord length c; therefore, the momentum loss per unit blade surface area is represented herein by $\theta_{tot}/2c$. This use of the blade chord length instead of the mean camber length affects only the magnitude of the momentum loss per unit surface area and in no way affects the results of the analysis presented herein.

[redacted]

The viscous loss along a blade surface depends on the velocities and flow conditions along the surface. Reference 2 shows that the momentum thickness at any point along the blade surface can be expressed by the following equation, which is equation (6) of reference 2 rewritten with the symbols of this report:

$$\theta_l = \frac{0.231}{\left[\left(\frac{\rho W}{\rho'' W_{cr}}\right)_{fs}\left(\frac{W}{W_{cr}}\right)_{fs}^{(1+H)}\right]_l}\left\{\int_0^l \frac{\left[\left(\frac{\rho W}{\rho'' W_{cr}}\right)_{fs}\left(\frac{W}{W_{cr}}\right)_{fs}^{1+H}\right]^{1.268}\left(\frac{\mu}{\rho W}\right)_{fs}^{0.268} K\, dl}{10^{0.678(2n+1)}}\right\}^{0.7886} \tag{1}$$

where

$$K = \left[1 - \frac{\gamma - 1}{\gamma + 1}\left(\frac{W}{W_{cr}}\right)_{fs}^2\right]^{0.467}$$

$$\frac{l}{n} = 2.6\, Re_{fs,l}^{1/14}$$

The free-stream Reynolds number $Re_{fs,l}$ at any point along the blade surface is based on the surface length from the leading edge to the point in question. The form factor H is the compressible-flow form factor.

For variations in blade geometry that do not affect the velocity distribution along the blade surfaces, equation (1) shows that

$$\frac{\theta}{c} \sim Re_{c,fs}^{-0.211} \tag{2}$$

where the chord length c is again used to approximate the blade surface length. The exponent of -0.211 agrees closely with the exponent of -1/5 that is commonly used in discussing viscous losses of turbulent boundary layers (e.g., refs. 5 and 6). In the following development, the momentum loss per unit blade surface area is assumed to vary in a manner similar to that based on one surface only, as in equation (2), so that

$$\frac{\theta_{tot}}{2c} \sim Re_c^{-m} \tag{3}$$

where

$$Re_c = \frac{\rho W c}{\mu} \tag{4}$$

In the calculations of values used in the figures of this report, the value of m is assumed equal to $1/5$.

For variations in blade geometry that do affect the surface velocity distribution, such as a change in channel shape for a given solidity or a change in the solidity itself, equation (1) shows that the value of the momentum thickness for each surface will change, and thus the total momentum thickness θ_{tot} will change. Therefore, even though the blade number and blade chord are specified, there can be a multitude of values of θ_{tot} for a given velocity diagram.

To understand the changes in total momentum thickness with changes in velocity distribution, first consider a blade of minimum solidity that would have high blade loading. Such a blade could have a high velocity level on both surfaces as a result of both a low solidity and a channel designed for high velocities on both surfaces. In this case, the momentum loss per unit blade surface area $\theta_{tot}/2c$ would be high. Next, consider a blade of almost infinite solidity for which the velocities on both surfaces would approach those of the axisymmetric solution. In this case, the momentum loss per unit blade surface area $\theta_{tot}/2c$ would approach a constant. Between these two extremes of solidity, the value of $\theta_{tot}/2c$ depends not only on the solidity but also on the surface velocity distribution for each solidity.

In addition to the velocity level on the blade surfaces, the static-pressure variation along the blade surface must also be considered. For instance, as the solidity is decreased, the loading per blade must increase to maintain the same velocity diagram; and, as blade loading increases, the static-pressure difference between the two surfaces also increases. If the static pressure on the suction surface decreases below that at the blade exit, then a static-pressure rise must occur, causing the boundary layer to thicken rapidly and possibly separate from the surface. (This boundary-layer condition is known as surface diffusion.) If the static pressure on the pressure surface rises above the static pressure at the blade inlet, then a surface diffusion would occur on the pressure surface. Thus, it can be seen that for a given solidity a wide range of blade losses could occur, depending on the amount of surface diffusion that is allowed to occur and on which surface the diffusion takes place.

In view of the multitude of values of $\theta_{tot}/2c$ that could exist for a given solidity, it is necessary to define which values should be used for each value of solidity; otherwise, an expression of $\theta_{tot}/2c$ as a function of solidity would be impossible. In an analysis of this sort, the minimum momentum loss per unit blade surface area for a given solidity and velocity diagram should be used. With the design procedures of references 7 and 8, the authors feel that it is possible to control the surface velocities at design operating conditions to attain close to a minimum momentum loss per unit blade surface area. With the surface velocities thus controlled, it seems reasonable that $\theta_{tot}/2c$ can be expressed as a function of solidity.

With the preceding stipulation on the momentum loss per unit blade surface area, for a given solidity the value of $\theta_{tot}/2c$ for one value of the blade chord length c can be related to that for a reference value of blade chord length by equation (3), which shows that

$$\frac{\theta_{tot}}{2c} = \left(\frac{\theta_{tot}}{2c}\right)_{ref}\left(\frac{Re_{c,ref}}{Re_c}\right)^m \tag{5}$$

In a two-dimensional cascade such as shown in figure 2, the blade loss can be described by a momentum-thickness parameter $\theta^*_{2\text{-}D}$, which represents the tangential projection of θ_{tot} divided by the blade spacing (see ref. 1), or

$$\theta^*_{2\text{-}D} = \frac{\theta_{tot}}{s \cos \beta_1}$$

which modified is

$$\theta^*_{2\text{-}D} = \left(\frac{\theta_{tot}}{2c}\right)\frac{2c}{s \cos \beta_1} \tag{6}$$

Substituting equation (5) into equation (6) and simplifying give

$$\theta^*_{2\text{-}D} = \left(\frac{\theta_{tot}}{c}\right)_{ref}\left(\frac{Re_{c,ref}}{Re_c}\right)^m \frac{c}{s \cos \beta_1} \tag{7}$$

For the three-dimensional case of turbomachines, the inner and outer walls also contribute to the viscous loss of a blade row; therefore, a three-dimensional analysis must be considered that includes the wall effect. Reference 3 shows that the three-dimensional loss can be satisfactorily predicted from the two-dimensional loss based on mean-section conditions by the following relation:

$$\theta^*_{3\text{-}D} = \theta^*_{2\text{-}D}\left(1 + \frac{\cos \alpha_s}{\sigma \mathscr{A}}\right) \tag{8}$$

where α_s is the blade stagger angle, σ is the blade solidity, and $\mathscr{A}$ is the aspect ratio. Then, substituting equation (7) into equation (8) and replacing $\sigma\mathscr{A}$ by its equivalent, b/s, result in

$$\theta^*_{3\text{-}D} = \left(\frac{\theta_{tot}}{c}\right)_{ref}\left(\frac{Re_{c,ref}}{Re_c}\right)^m\left(\frac{c}{s \cos \beta_1}\right)\left(1 + \frac{\cos \alpha_s}{b/s}\right) \tag{9}$$

Substituting equation (4) into equation (9) gives

$$\theta^*_{3\text{-}D} = \left(\frac{\theta_{tot}}{c}\right)_{ref}\left(\frac{Re_{c,ref}}{\frac{\rho W}{\mu}}\right)^m\left(\frac{c^{1-m}}{s \cos \beta_1}\right)\left(1 + \frac{\cos \alpha_s}{b/s}\right) \tag{10}$$

To organize equation (10) a little differently, let

$$\frac{c^{1-m}}{s} = \left(\frac{c}{s}\right)^{1-m}\left(\frac{s}{b}\right)^{-m} b^{-m} \tag{11}$$

Then, substituting equation (11) into equation (10), σ for c/s, and rearranging the terms give

$$\theta^*_{3\text{-}D} = \underbrace{\left(\frac{b}{s}\right)^m\left(1 + \frac{\cos \alpha_s}{b/s}\right)}_{f\left(\frac{b}{s}\right)}\underbrace{\left(\frac{\theta_{tot}}{c}\right)_{ref} \sigma^{1-m}}_{f(\sigma)}\underbrace{Re_b^{-m}}_{f(Re_b)}\frac{Re^m_{c,ref}}{\cos \beta_1} \tag{12}$$

A B C

By arranging the terms in equation (12) as shown above, the viscous loss for a given velocity diagram, as represented here by a three-dimensional momentum-thickness parameter, is shown to be a function of three variables, the blade height-to-spacing ratio b/s, the blade mean-section solidity σ, and a Reynolds number based on blade height Re_b (hereinafter called a height Reynolds number). Examples of the changes in blade shape for each of these variables are given in figure 3. The effect of the change of each variable is determined in the remainder of the analysis and is discussed in the RESULTS OF ANALYSIS.

It should be noted that the blade stagger angle α_s and the blade outlet relative gas-flow angle β_1 are largely dependent on the velocity

diagram and are approximately constant for a particular application; therefore, they are considered to be constant for each set of design conditions.

With regard to stating $(\theta_{tot}/c)_{ref}$ as a function of solidity σ in equation (12), it should be remembered that, according to previous stipulations, there is considered to be only one value of θ_{tot}/c for each value of solidity based on the minimum momentum loss per unit blade surface area for a given solidity and velocity diagram.

Determination of Optimum Blade Geometry

Equation (12) shows that the viscous loss of a blade row is a function of three independent variables, the blade height-to-spacing ratio b/s, the solidity σ, and the height Reynolds number Re_b. Because of the independence of these three variables, an optimum value of the momentum-thickness parameter θ^*_{3-D} can be determined by optimizing each variable separately. Also, the effect of each variable on θ^*_{3-D} can be studied independently.

Blade height-to-spacing ratio and related parameters. - For a decrease in the blade height-to-spacing ratio b/s resulting from a change in blade spacing s (holding solidity σ and height Reynolds number Re_b constant) as shown in figure 3(a), the total surface area of all the blades does not change, but both the chord length and end-wall areas increase. As the chord length becomes longer, the chord Reynolds number Re_c increases. Thus, by equation (3) the momentum loss per unit blade surface area decreases. Counteracting the effect of this reduction in the momentum loss per unit surface area is the increase in end-wall area over which the momentum loss occurs. This counteraction indicates the possibility of obtaining some optimum value of b/s (or, in effect, an optimum number of blades) which would be required to give a minimum value of blade viscous loss.

To determine a minimum value of θ^*_{3-D} as a function of the blade height-to-spacing ratio b/s (holding σ and Re_b constant as indicated by subscripts on the partial derivative), let

$$\left[\frac{\partial\theta^*_{3-D}}{\partial\left(\frac{b}{s}\right)}\right]_{\sigma,Re_b} = \frac{dA}{d\left(\frac{b}{s}\right)} = 0$$

From equation (12),

$$\frac{dA}{d\left(\frac{b}{s}\right)} = m\left(\frac{b}{s}\right)^{m-1} + \cos \alpha_s (m - 1)\left(\frac{b}{s}\right)^{m-2}$$

The value of the optimum blade height-to-spacing ratio can then be expressed as

$$\left(\frac{b}{s}\right)_{opt} = \left(\frac{1}{m} - 1\right)\cos \alpha_s \tag{13}$$

Because the value of m can be assumed equal to $1/5$, the value of $(b/s)_{opt}$ is thus determined by the stagger angle α_s, which itself is approximately specified by the blade velocity diagram (see appendix B). Therefore, on the basis of the velocity diagram alone, an optimum blade height-to-spacing ratio can be determined.

In order that the results of the preceding analysis can be interpreted in terms of the blade number N and the aspect ratio $\mathscr{A}$, let

$$b = r_t - r_h = r_t\left(1 - \frac{r_h}{r_t}\right) \tag{14}$$

and

$$s = \frac{2\pi r_m}{N} = \frac{\pi r_t}{N}\left(1 + \frac{r_h}{r_t}\right) \tag{15}$$

Dividing equation (14) by equation (15) gives

$$\frac{b}{s} = \frac{N}{\pi}\left(\frac{1 - \frac{r_h}{r_t}}{1 + \frac{r_h}{r_t}}\right) \tag{16}$$

Now, since the hub-tip radius ratio is specified by the velocity diagram and since $(b/s)_{opt}$ is known from equation (13), then the optimum number of blades for these conditions and a constant hub-tip ratio from blade inlet to outlet can be obtained from the following rearranged form of equation (16):

$$N_{opt} = \pi\left(\frac{b}{s}\right)_{opt}\left(\frac{1 + \frac{r_h}{r_t}}{1 - \frac{r_h}{r_t}}\right)$$

or from its equivalent form

$$N_{opt} = \pi\left(\frac{1}{m} - 1\right)\cos \alpha_s \left(\frac{1 + \frac{r_h}{r_t}}{1 - \frac{r_h}{r_t}}\right) \tag{17}$$

Curves of N_{opt} as a function of r_h/r_t for a range of values of α_s are shown in figure 4 for an m of 1/5.

The value of the optimum blade height-to-spacing ratio determined by equation (13) corresponds to a particular value of the product of the solidity σ and the aspect ratio $\mathscr{A}$, as shown by

$$\left(\frac{b}{s}\right)_{opt} = \left(\frac{c}{s}\frac{b}{c}\right)_{opt} = (\sigma\mathscr{A})_{opt} \tag{18}$$

Equation (18) can be interpreted to mean that for a given velocity diagram and a given solidity there is a value of the aspect ratio which will result in a minimum viscous loss for the given conditions. Figure 5 shows such values of aspect ratio over a range of solidities and velocity diagrams (as shown by the stagger angle α_s). If the optimum solidity is known or estimated from appendix B, then an optimum aspect ratio can be determined.

Solidity. - For an increase in solidity σ (holding the blade height-to-spacing ratio b/s and height Reynolds number Re_b constant), the blade chord length c and the surface areas of both the blade and end walls increase as shown in figure 3(b). The momentum loss per unit surface area $\theta_{tot}/2c$ decreases as a result of both a decrease in the blade loading (which decreases the velocities on the blade surfaces, as discussed previously) and the effect of an increase in the chord Reynolds number (see eq. (3)). Counteracting this reduction in the momentum loss per unit surface area is an increase in the total blade surface and end-wall area over which the momentum loss occurs. This counteraction indicates the possibility of obtaining an optimum solidity that would result in a minimum value of blade viscous loss.

To determine a minimum value of viscous loss with respect to solidity (holding b/s and Re_b constant), let

$$\left(\frac{\partial \theta^*_{3\text{-}D}}{\partial \sigma}\right)_{b/s,Re_b} = \frac{dB}{d\sigma} = 0$$

From equation (12),

$$\frac{dB}{d\sigma} = \left(\frac{\theta_{tot}}{c}\right)_{ref} (1 - m)\, \sigma^{-m} + (\sigma^{1-m}) \frac{d\left(\frac{\theta_{tot}}{c}\right)_{ref}}{d\sigma} \tag{19}$$

The value of the optimum solidity can then be expressed as

$$\sigma_{opt} = (1 - m)\left(\frac{\theta_{tot}}{c}\right)_{ref,opt}\left[-\frac{d\sigma}{d\left(\frac{\theta_{tot}}{c}\right)_{ref}}\right]_{opt} \tag{20}$$

A method of determining the optimum solidity is to rearrange equation (20) as follows:

$$\left(\frac{d\sigma}{\sigma}\right)_{opt} = -\left(\frac{1}{1 - m}\right)\left[\frac{d\left(\frac{\theta_{tot}}{c}\right)_{ref}}{\left(\frac{\theta_{tot}}{c}\right)_{ref}}\right]_{opt}$$

and to express it as

$$d(\ln \sigma_{opt}) = -\left(\frac{1}{1 - m}\right) d\left[\ln\left(\frac{\theta_{tot}}{c}\right)_{ref,opt}\right]$$

Then, by further rearrangement,

$$\frac{d\left[\ln\left(\frac{\theta_{tot}}{c}\right)_{ref,opt}\right]}{d(\ln \sigma_{opt})} = -(1 - m) \tag{21}$$

Therefore, if $(\theta_{tot}/c)_{ref}$ is plotted as a function of solidity σ on logarithmically scaled paper, the optimum solidity σ_{opt} can be determined by the point where the slope of a tangent to the curve is equal to $-(1 - m)$, as in figure 6 for the example turbines.

Height Reynolds number. - The height Reynolds number Re_b can change as a result of both a change in blade height and a change in the blade inlet flow conditions. In the following development, only the change in height Reynolds number resulting from a change in blade height is considered. The effect of a change in height Reynolds number resulting from a change in the inlet flow conditions is discussed in the section entitled RESULTS OF ANALYSIS.

The turbine design conditions that remain constant during a change in height Reynolds number resulting from a change in blade height only are the hub-tip radius ratio, the rotor tip speed, and the velocity diagrams at corresponding radial positions. In order to hold these conditions constant, the weight flow and annulus area must vary as the square of the tip diameter.

For an increase in Re_b as prescribed (holding the blade height-to-spacing ratio b/s and solidity σ constant, fig. 3(c)), the total end-wall and blade surface areas increase as the square of the tip diameter, and the chord length c increases directly as the blade height (or tip diameter). The increase in the blade chord length c results in an increase in the chord Reynolds number Re_c, which results in a reduction in the momentum loss per unit surface area (see eq. (3)). For the specified increase in Re_b, the weight flow and total surface area increase proportionally; therefore, on the basis of the momentum loss per unit of free-stream momentum, the effect of the increase in chord Reynolds number on the reduction of the momentum loss per unit surface area is not counteracted by the increase in total surface area as in the case of changes in the blade height-to-spacing ratio b/s and solidity σ. Then, as the blade height Reynolds number increases, the viscous losses as defined by the momentum-thickness parameter $\theta^*_{3\text{-}D}$ would decrease; and, since there is no counteracting effect of a change in surface area, there will be no optimum value of the height Reynolds number.

To verify the preceding discussion mathematically, letting Re_b vary and holding b/s and σ constant, set

$$\left(\frac{\partial \theta^*_{3\text{-}D}}{\partial Re_b}\right)_{b/s,\sigma} = \frac{dC}{dRe_b} = 0 \tag{22}$$

From equation (12),

$$\frac{dC}{dRe_b} = -mRe_b^{-m-1}$$

For equation (22) to be true, the value of Re_b must approach infinity; therefore, there is no minimum value of $\theta^*_{3\text{-}D}$ obtainable for changes in Re_b only.

Effect of Changing Blade Geometry

Sometimes a compromise has to be made between aerodynamic efficiency and mechanical considerations; therefore, it is important to know what penalty is paid in performance by deviating from an optimum blade configuration. In the following sections the difference in the loss for a given blade configuration and that for an optimum or reference configuration is indicated by the ratio of a momentum-thickness parameter to either a minimum or reference momentum-thickness parameter. The changes in geometry that are studied are defined by the three primary variables previously considered, namely, the blade height-to-spacing ratio b/s, solidity σ, and height Reynolds number Re_b, where the blade inlet flow conditions are considered to be constant.

4061

Blade height-to-spacing ratio. - From equation (12), the change in the value of the momentum-thickness parameter with a change in the blade height-to-spacing ratio b/s for a given velocity diagram (holding the solidity σ and height Reynolds number Re_b constant) as shown in figure 3(a) can be expressed by

$$\left(\frac{\theta^*_{3\text{-}D}}{\theta^*_{3\text{-}D,min}}\right)_{\sigma,Re_b} = \frac{\left(\frac{b}{s}\right)^m\left(1 + \frac{\cos \alpha_s}{b/s}\right)}{\left(\frac{b}{s}\right)^m_{opt}\left[1 + \frac{\cos \alpha_s}{(b/s)_{opt}}\right]} \tag{23}$$

Having prescribed the blade height b constant by assuming a constant value of the height Reynolds number Re_b as discussed previously, then, for a given hub-tip ratio,

$$\frac{\frac{b}{s}}{\left(\frac{b}{s}\right)_{opt}} = \frac{N}{N_{opt}} \tag{24}$$

which, rearranged, is

$$\frac{b}{s} = \left(\frac{b}{s}\right)_{opt}\frac{N}{N_{opt}} \tag{25}$$

Substituting equation (13) into equation (25) gives

$$\frac{b}{s} = \left(\frac{1}{m} - 1\right) \cos \alpha_s \cdot \frac{N}{N_{opt}} \tag{26}$$

Then, substituting equations (13) and (26) into equation (23) and simplifying give

$$\left(\frac{\theta^*_{3\text{-}D}}{\theta^*_{3\text{-}D,min}}\right)_{\sigma,Re_b} = \left(\frac{N}{N_{opt}}\right)^m \left\{1 + m\left[\left(\frac{N}{N_{opt}}\right)^{-1} - 1\right]\right\} \tag{27}$$

The variation of the momentum-thickness parameter with the number of blades as given in equation (27) is shown by figure 7(a) and is discussed in the RESULTS OF ANALYSIS.

Solidity. - From equation (12), the change in the value of the momentum-thickness parameter with a change in solidity σ for a given velocity diagram (holding the blade height-to-spacing ratio b/s and height Reynolds number Re_b constant) as shown in figure 3(b) can be expressed by

$$\left(\frac{\theta^*_{3\text{-}D}}{\theta^*_{3\text{-}D,min}}\right)_{b/s,Re_b} = \frac{\left(\frac{\theta_{tot}}{c}\right)_{ref} \sigma^{1-m}}{\left(\frac{\theta_{tot}}{c}\right)_{ref,opt} \sigma_{opt}^{1-m}} \tag{28}$$

Values of $(\theta_{tot}/c)_{ref}$ could be obtained from a curve of θ_{tot}/c as a function of σ such as figure 6. The curve in figure 6 is based on the experimental performance of four turbine rotors differing only in solidity. The method for obtaining the value of θ_{tot}/c for each rotor is discussed in connection with the DESCRIPTION OF EXAMPLE TURBINES.

From figure 6, values of $(\theta_{tot}/c)/(\theta_{tot}/c)_{opt}$ were calculated for a range of values of σ/σ_{opt}, assuming that the optimum values correspond to the point where the slope of the curve is equal to $-(1 - m)$ as previously discussed. Then, by substituting these values into equation (28) and using an m of 1/5, corresponding values of $\theta^*_{3\text{-}D}/\theta^*_{3\text{-}D,min}$ were calculated. The variation of $\theta^*_{3\text{-}D}/\theta^*_{3\text{-}D,min}$ with σ/σ_{opt} is shown in figure 7(b) and is discussed later in the RESULTS OF ANALYSIS.

Blade height-to-spacing ratio and solidity combined. - For a given velocity diagram, the effect of varying the blade height-to-spacing ratio

(or blade number) and solidity (holding the height Reynolds number Re_b constant) can be determined by superimposing the effect of one upon the other. From equations (27) and (28),

$$\left(\frac{\theta^*_{3\text{-}D}}{\theta^*_{3\text{-}D,min}}\right)_{Re_b} = \left(\frac{N}{N_{opt}}\right)^m \left\{1 + m\left[\left(\frac{N}{N_{opt}}\right)^{-1} - 1\right]\right\}\left[\frac{\left(\frac{\theta_{tot}}{c}\right)_{ref} \sigma^{1-m}}{\left(\frac{\theta_{tot}}{c}\right)_{ref,opt} \sigma_{opt}^{1-m}}\right] \quad (29)$$

Because the effects of varying the blade height-to-spacing ratio and solidity are represented by a product in equation (29), the effect of varying one of these two variables, holding the other variable at some value other than optimum, is to increase by a constant multiplier the amount of the change of $\theta^*_{3\text{-}D}/\theta^*_{3\text{-}D,min}$ with the chosen variable. For example, for a constant $N/N_{opt} \gtrless 1.0$ the effect of a solidity variation on $\theta^*_{3\text{-}D}/\theta^*_{3\text{-}D,min}$ is magnified by the value of $\theta^*_{3\text{-}D}/\theta^*_{3\text{-}D,min}$ calculated by equation (27) for the particular value of N/N_{opt}. A similar effect on the variation of $\theta^*_{3\text{-}D}/\theta^*_{3\text{-}D,min}$ with N/N_{opt} exists for $\sigma/\sigma_{opt} \gtrless 1.0$. The combination of the effects of changes in blade number and solidity on the value of $\theta^*_{3\text{-}D}/\theta^*_{3\text{-}D,min}$ is shown in figure 7(c) and is discussed later in the RESULTS OF ANALYSIS.

Aspect ratio. - In order to determine the variation in the momentum-thickness parameter with changes in aspect ratio for a given velocity diagram (holding the height Reynolds number Re_b constant), substitute equation (18) into equation (24) as follows:

$$\frac{\frac{b}{s}}{\left(\frac{b}{s}\right)_{opt}} = \frac{N}{N_{opt}} = \frac{\mathscr{A}\sigma}{(\mathscr{A}\sigma)_{opt}} \quad (30)$$

Then, on the basis of the discussion of equation (18), for an optimum value of solidity, an optimum aspect ratio can be determined. Then, assuming an optimum solidity for the condition of an optimum blade height-to-spacing ratio, equation (30) can be rearranged in the following form:

$$\frac{\sigma}{\sigma_{opt}} = \left(\frac{\mathscr{A}}{\mathscr{A}_{opt}}\right)^{-1} \frac{N}{N_{opt}} \quad (31)$$

Now, if $\mathscr{A}/\mathscr{A}_{opt}$ is assumed to be constant, then equation (31) represents the equation of a straight line through the origin with a slope of $(\mathscr{A}/\mathscr{A}_{opt})^{-1}$. Such lines of constant $\mathscr{A}/\mathscr{A}_{opt}$ are shown on figure 7(c), and they indicate the variation of $\theta^*_{3\text{-}D}/\theta^*_{3\text{-}D,min}$ for blades of constant height and constant chord length, but varying blade number and solidity.

Height Reynolds number. - As previously discussed, there is no optimum value of the height Reynolds number Re_b obtainable; therefore, the variation of the momentum-thickness parameter with a change in Re_b for a given velocity diagram (holding the blade height-to-spacing ratio b/s and solidity σ constant) is based on a specified, or reference, value of Re_b as in the following equation:

$$\left(\frac{\theta^*_{3\text{-}D}}{\theta^*_{3\text{-}D,ref}}\right)_{b/s,\sigma} = \left(\frac{Re_b}{Re_{b,ref}}\right)^{-m} \tag{32}$$

For constant inlet flow conditions, equation (32) can be expressed as

$$\left(\frac{\theta^*_{3\text{-}D}}{\theta^*_{3\text{-}D,ref}}\right)_{b/s,\sigma} = \left(\frac{b}{b_{ref}}\right)^{-m}$$

As shown by equation (32), the momentum-thickness parameter $\theta^*_{3\text{-}D}$ varies as the $-m$ power of the height Reynolds number for the conditions specified. This variation of $\theta^*_{3\text{-}D}$ with Re_b is shown in figure 7(d) and is discussed in the RESULTS OF ANALYSIS.

DESCRIPTION OF EXAMPLE TURBINES

The four turbines chosen for use in the development of the analysis of this report have been previously reported in reference 9. Also discussed is a fifth turbine reported in reference 10. All five turbines are briefly discussed herein, and some of the geometric and performance variables are given in table I. More complete descriptions of the designs and test results are given in references 9 and 10.

The four turbines of reference 9 differed in the number of rotor blades only, and they consisted of 64, 44, 32, and 24 blades. The blade shapes were the same for each number of blades; and, to change the blade spacing for different numbers of blades, spacers were placed between the blade bases. It should be noted that the variation in number of blades

results in a variation of solidity without a subsequent change in blade profile to control the blade surface velocities. In spite of this, low surface diffusions probably occurred because the flow within the rotor passage turned through an angle of only 51° at the mean section. Therefore, the four turbines of reference 9 should yield a variation of blade viscous loss that is fairly representative of the values of minimum viscous loss for each value of solidity.

The example turbines had a tip diameter of 14 inches and a hub-tip ratio of 0.6. The chord setting angle of all the rotor blades was 28°. The blade-section coordinates for the 88-blade rotor were half those for the 44-blade rotor. For each of the five turbines, the same stator blades were used.

The viscous loss calculated for the five turbine rotors was based on an effective momentum thickness $\overline{\theta}_{tot}$ calculated for each of the rotors by the method given in reference 4. The effective momentum thickness for each rotor was determined from a rotor loss total-pressure ratio based on experimental performance data obtained at design operating conditions. In order to calculate the rotor loss total-pressure ratio, it was necessary to determine the turbine over-all total-pressure ratio at design specific work and speed by interpolating between total-pressure-ratio contours shown on an experimentally obtained performance map. It was also necessary to obtain a value of loss total-pressure ratio for the stator used.

The design-point efficiency based on the interpolated value of total-pressure ratio can be calculated to three decimal places with only a probable error of about 1 in the third place due to the interpolation. Although the absolute value of efficiency to this degree of accuracy is questionable, the trend of the rotor viscous loss based on the performance maps of the five turbines should be fairly accurate, because the same test facility, instrumentation, and procedure were used for each turbine. The variation in design-point efficiency of the four turbines of reference 9 is presented as a function of solidity σ in figure 8. If figure 8 is compared with figure 6(a) of reference 9, it should be noted that reference 9 compares the four turbines on the basis of a maximum efficiency and a solidity based on the axial blade chord length. Therefore, the values in figure 8 are not equal to those in figure 6(a) of reference 9.

RESULTS OF ANALYSIS

In previous sections, the variation of viscous loss with changes in blade geometry has been developed. The principal variables that were found to have a direct effect on the viscous loss for a given velocity

diagram are the blade height-to-spacing ratio b/s, the solidity σ, and the height Reynolds number Re_b. The results of the previous analysis and the significance of each of these variables are discussed below. Since the trailing-edge blockage also affects the over-all blade loss after mixing, a brief account of its effect on the selection of the number of blades that will result in the minimum over-all blade loss will be discussed in connection with the effect of the blade height-to-spacing ratio.

Blade Height-to-Spacing Ratio

As pointed out previously, the effect of varying the blade height-to-spacing ratio (holding the solidity σ and height Reynolds number Re_b constant) as shown in figure 3(a) results in a chord Reynolds number effect on the momentum loss per unit surface area, which is counteracted by a change in the area of the end walls, while the total blade-surface area remains constant. These counteracting effects are shown by figure 7(a) to counterbalance each other over a wide range of blade-number ratio N/N_{opt}, especially at blade numbers greater than the optimum. For example, over a range of N/N_{opt} from 0.37 to 2.60 (a change in blade number of about 7 to 1) the change in the momentum-thickness parameter never exceeds 10 percent of the minimum value. A similar result is shown in figure 48 of reference 11, which gives the variation in compressor efficiency with the number of blades.

This insensitivity of blade loss to a change in number of blades is also indicated by the experimental and predicted losses of the 88-blade rotor of reference 10 and the 44-blade rotor of reference 9. Both of these rotors were designed for the same solidity, blade height, and stagger angle and operated at similar inlet flow conditions. Therefore, the fundamental difference between the rotors was the number of blades (or aspect ratio). Comparing the design-point efficiencies determined by the method of interpolation discussed in the DESCRIPTION OF EXAMPLE TURBINES shows that the efficiency of 0.887 for the 88-blade rotor is slightly less than the 0.891 for the 44-blade rotor. These two values of efficiency can be considered equal considering the possible experimental error; however, it is interesting to compare this small change in efficiency with the predicted change in the rotor blade viscous loss as indicated by figure 7(c). The optimum values of blade number and solidity used in determining the location of the data points for the two rotors in figure 7(c) were based on the optimum values predicted in the METHOD OF ANALYSIS. The data point for the 44-blade rotor is on an $\mathscr{A}/\mathscr{A}_{opt}$ line of 0.9 and in a region of $\theta^*_{3\text{-}D}/\theta^*_{3\text{-}D,min}$ less than 1.01, and the data point for the 88-blade rotor is on an $\mathscr{A}/\mathscr{A}_{opt}$ line of 1.8 and in a

region of $\theta^*_{3\text{-}D}/\theta^*_{3\text{-}D,min}$ of about 1.038. This small difference in the momentum-thickness-parameter ratio indicates that the 88-blade rotor would have a slightly higher viscous loss than the 44-blade rotor. Comparison of this result with the small difference in design-point efficiencies shows that the slight increase in viscous loss agrees with the slight decrease in efficiency. This comparison and results discussed later indicate that for the five example turbines an increase in $\theta^*_{3\text{-}D}/\theta^*_{3\text{-}D,min}$ of 0.01 corresponds to a decrease in efficiency of about 0.001.

Because the four turbines of reference 9 have the same aspect ratio, their values would be located on the constant $\mathscr{A}/\mathscr{A}_{opt}$ line through the data point for the 44-blade rotor shown in figure 7(c). The experimental variation of θ_{tot}/c with σ used to obtain this figure is represented by the variation of $\theta^*_{3\text{-}D}/\theta^*_{3\text{-}D,min}$ along this constant $\mathscr{A}/\mathscr{A}_{opt}$ line.

In the method presented for determining the optimum number of blades for a given velocity diagram, the losses associated with the trailing-edge blockage were assumed to be constant. If, however, the trailing-edge thickness cannot be reduced as the blade number is increased, the trailing-edge blockage must increase with an increase in the number of blades. Although the magnitude of the change in over-all blade loss with a change in trailing-edge blockage cannot be accurately determined by theory, the trend of the changes can be obtained from the theory. For example, the results of a series of calculations made for the stator of reference 8 by the method given in appendix C are shown in figure 9. In this figure, the variation in the loss total-pressure ratio p'_2/p'_0 represents the variation in the over-all blade loss after mixing.

In figure 9, the values shown for zero trailing-edge thickness represent the variation in the over-all blade viscous loss with changes in blade number similar to that shown in figure 7(a). For a given blade number, the difference between the loss at any given trailing-edge thickness and that at zero trailing-edge thickness represents the contribution of the trailing-edge blockage to the over-all blade loss.

The two circled points in figure 9 represent results for the same trailing-edge blockage but for different blade numbers and trailing-edge thicknesses, namely, 40 blades with 0.050-inch-thick trailing edges and 80 blades with 0.025-inch-thick trailing edges. The difference between the loss total-pressure ratios for trailing-edge thicknesses of zero and 0.050 inch for 40 blades is equal to the difference in loss total-pressure ratios for trailing-edge thicknesses of zero and 0.025 inch for 80 blades. Similar comparisons can be made elsewhere on the figure; therefore, the assumption that the loss associated with the trailing-edge

blockage is constant for a constant trailing-edge blockage but varying blade number seems to be valid for a specified velocity diagram.

As an example of the variation of over-all blade loss with a change in trailing-edge blockage, consider the curve in figure 9 for a constant trailing-edge thickness of 0.050 inch. This curve indicates a change in the loss total-pressure ratio from 0.9535 to 0.9695 with a change from 60 to 23 blades. Comparing this variation with that for zero trailing-edge thickness indicates that the loss associated with trailing-edge blockage may be high and that this loss should be considered in selecting the number of blades corresponding to the minimum over-all blade loss.

It should be noted that the optimum number of blades decreases with increases in the trailing-edge thickness. For example, figure 9 indicates that the optimum numbers of blades for trailing-edge thicknesses of 0, 0.010, 0.025, and 0.050 inch are 46, 38, 30, and 23, respectively. Therefore, the use of figure 4 in determining the optimum number of blades is only applicable when considering a constant trailing-edge blockage and not when considering a constant trailing-edge thickness. Because variations in trailing-edge blockage affect the value of the blade number corresponding to a minimum over-all blade loss, it is necessary to determine the optimum number of blades for a specified trailing-edge thickness by considering both changes in the blade viscous loss and the loss associated with the trailing-edge blockage. This can be done by determining the values of the loss total-pressure ratio for a given trailing-edge thickness over a range of blade numbers by the method given in appendix C and then selecting the blade number corresponding to the maximum loss total-pressure ratio.

It should also be noted from figure 9 that, for a change in the trailing-edge thickness from zero to 0.050 inch, the maximum loss total-pressure ratio changes from 0.9735 to 0.9695. Therefore, if thick trailing edges are required, little penalty will be paid if the blade number is reduced to correspond to the minimum over-all blade loss for the trailing-edge thickness required.

Solidity

It was pointed out in the analysis that varying the solidity (holding the blade height-to-spacing ratio b/s and the height Reynolds number Re_b constant) as shown in figure 3(b) results in a change in the blade chord length and the surface areas of both the blade and end walls. It was also noted that the momentum loss per unit surface area changes with solidity as a result of the effects of a change in the chord Reynolds number and the blade surface velocity distribution, and that a change in the viscous loss as a result of a change in momentum

[redacted]

loss per unit surface area is counteracted by a change in the blade surface and end-wall areas. These counteracting effects are shown by figure 7(b) to counterbalance each other over a range of solidities from about σ/σ_{opt} of 0.73 to 1.31 (or a change of about 2 to 1), where the change in the momentum-thickness parameter never exceeds 10 percent of the minimum value. This variation in the viscous loss with solidity can be compared with the variation in efficiency for the example turbines shown in figure 8. For example, from a solidity of 1.20 to 2.25, with an optimum indicated at about 1.65, the efficiency remains within 0.01 of the maximum efficiency. A similar wide range of solidities with little effect on design-point performance is also indicated by the transonic turbine rotors of references 7 and 12. The rotor of reference 7 had a solidity of 1.86 with a design-point efficiency of 0.869, and the rotor of reference 12 had a solidity of 2.86 with an efficiency of 0.872.

4061

A comparison of the variations of the momentum-thickness parameter with blade number and solidity as shown in figures 7(a) and (b) indicates that the viscous loss is more sensitive to changes in solidity than it is to the number of blades. This is especially true when comparing the values of the momentum-thickness-parameter ratio at greater than optimum values of solidity and blade number. This difference in the variations of viscous loss with solidity and blade number can be explained by the fact that the blade surface area changes with solidity but is constant as the blade number changes. Thus, the effect of a change in the momentum loss per unit surface area is offset more by changes in area with changes in solidity than it is with changes in area due to changes in the number of blades alone.

Considerable effort has been made to provide some means for estimating an optimum blade solidity for a particular velocity diagram (see refs. 5, 9, and 13). It should be noted that Zweifel's method (ref. 13) is developed for incompressible and frictionless flow through a two-dimensional cascade and is based on the assumption of zero suction-surface diffusion in the case of reaction blade rows. For three-dimensional blade rows for compressible flow with both high- and low-reaction blade rows and with zero suction-surface diffusion investigated by the authors, the optimum solidities indicated by the test results closely agree with those predicted by Zweifel's method based on blade chord instead of axial chord. (This slight change in Zweifel's method is discussed in appendix B.) For example, the optimum solidity based on Zweifel's method for the example turbines of this report is 1.55 as compared with the optimum solidity of about 1.65 indicated by the performance results (see fig. 8). Since a 30-percent variation from the optimum solidity results in less than 0.01 drop in efficiency, the optimum solidity predicted by figure 10, which is based on the development of appendix B, should result in efficiencies sufficiently close to the optimum.

Changes in Blade Height-to-Spacing Ratio and Solidity Combined

The variation of the momentum-thickness parameter with changes in both the number of blades and the solidity is indicated in figure 7(c). The area of the figure enclosed by the contour for $\theta^*_{3\text{-}D}/\theta^*_{3\text{-}D,min}$ of 1.10 approximately represents the region over which the difference between the optimum efficiency and the efficiency for any configuration within the region would be less than 0.01. It should be noted that this region covers a fairly large range of blade number and solidity; however, it is again evident that the blade loss is more sensitive to solidity than it is to the number of blades over the entire range of the figure.

Height Reynolds Number

The analysis showed that a change in the height Reynolds number for a given velocity diagram (holding the blade height-to-spacing ratio b/s and solidity σ constant) as shown in figure 3(c) results in a change in the blade surface and end-wall areas, the weight flow, and the blade chord length. It was pointed out, however, that only the change in blade chord length affects the viscous losses when considering the viscous loss per unit of free-stream momentum, and that there is no counterbalancing effect of area. Therefore, for every increase in the height Reynolds number either by varying the geometry or the inlet flow conditions there should be an improvement in blade performance, as shown by figure 7(d). It should be noted that the height Reynolds number is the only primary variable in equation (12) for which there is not an effect to counteract the effect of a change in chord Reynolds number.

The effects of turbine size and inlet flow conditions on turbine performance have been reported many times in the past. For instance, an improvement in performance with an increase in Re_b due to changes in inlet flow conditions only has been previously indicated by a series of tests on a single-stage turbine reported in reference 14. For changes in stator size only, figure 15(b) of reference 5 indicates that, for a constant aspect ratio and solidity, the stator blade loss decreases with increases in blade height or, in effect, the height Reynolds number.

For rotating blade rows, similarity is based not only on similar blade geometry and flow conditions but also on similar work output per unit of wheel speed. This principle of similarity for turbomachinery is discussed in detail in reference 15. The parameter often used to correlate the losses of turbomachines that are similar, as stated previously, is a machine Reynolds number that is defined in reference 15 as the product of the rotor tip speed and the tip diameter divided by the kinematic viscosity at inlet conditions. In this case, variations in the tip diameter represent changes in the scale of the turbine; therefore, changes in blade height would be proportional to changes in the

tip diameter. Thus, the same correlations of the performance of similar turbomachines would be obtained for both the machine and height Reynolds numbers. The main difference between the two is that, for two-dimensional or three-dimensional, stationary or moving blade rows, the height Reynolds number can be used; whereas, the machine Reynolds number applies specifically to rotating components.

The effect of the machine Reynolds number on the performance of a wide variety of turbomachines is presented in reference 16. This reference shows that for every turbomachine reported the performance improved as the machine Reynolds number increased. A similar trend is also reported in reference 11, which shows that compressor and turbine performance improves with an increase in the machine Reynolds number.

SUMMARY OF RESULTS

An analytical investigation of the effect of changing blade geometry on the viscous losses of axial-flow turbomachines has been presented. It was found that the viscous losses can be expressed as a function of three independent variables: blade height-to-spacing ratio, solidity, and height Reynolds number. For values of these variables for a series of turbines for the same velocity diagram, a method of approximately determining the optimum values of the blade number and solidity was derived on the basis of experimental data for four conservatively designed turbine rotors. The effects of deviating from these optimum values were also presented. Since changes in trailing-edge blockage also affect the blade loss total-pressure ratio, an analytical means of studying its effect on the number of blades corresponding to the minimum total-pressure loss was also given.

In studying the effects of changes in blade height-to-spacing ratio, solidity, height Reynolds number, and trailing-edge blockage on the over-all blade loss it was found that, for a change in each variable independent of the other three:

1. A change in blade number results in two counteracting effects resulting from changes in the chord Reynolds number and end-wall area. These two effects counterbalance each other fairly well over a wide range of blade number.

2. A change in solidity results in two counteracting effects due to a change in the momentum loss per unit surface area and a change in the area of the blade surfaces and the end walls. These effects counterbalance each other over a more limited range of solidity than is the case when only blade number is varied.

[redacted]

3. A change in the height Reynolds number, resulting from either a change in the inlet flow conditions or the scale of the turbine, results in a change in the viscous loss due to the effect of a change in the chord Reynolds number, and this effect is not counteracted by the change in the blade-surface and end-wall areas. Thus, an increase in the height Reynolds number results in an improvement in over-all performance. Furthermore, the height Reynolds number is an important parameter that should be considered in correlating the performance of different turbomachines.

4. The trailing-edge blockage may affect to some extent the choice of the number of blades corresponding to the minimum total-pressure loss. Also, the number of blades thus chosen will decrease with an increase in the trailing-edge thickness.

Lewis Flight Propulsion Laboratory
National Advisory Committee for Aeronautics
Cleveland, Ohio, June 22, 1956

[redacted]

APPENDIX A

SYMBOLS

A	function of blade height-to-spacing ratio in eq. (12)
$\mathscr{A}$	blade aspect ratio, b/c
B	function of solidity in eq. (12)
b	blade height, ft
C	function of height Reynolds number in eq. (12)
c	blade chord length at mean radius, ft
H	boundary-layer form factor, δ/θ
$\Delta h'$	specific work, Btu/lb
l	distance along blade surface measured from forward stagnation point, ft
m	exponent defining effect of change in Reynolds number on ratio of momentum thickness to chord
N	number of blades
n	exponent defining simple-power-law velocity profile, $\frac{W}{W_{fs}} = \left(\frac{Y}{\delta_f}\right)^n$
p	absolute pressure, lb/sq ft
Re_b	Reynolds number based on blade height, $\rho Wb/\mu$
Re_c	Reynolds number based on blade chord length, $\rho Wc/\mu$
r	radius, ft
s	blade spacing or pitch at mean radius, ft
t	blade trailing-edge thickness, ft
V	absolute gas velocity, ft/sec
W	relative gas velocity, ft/sec

Y length measured perpendicular to blade surface, ft

α absolute gas-flow angle measured from axial direction, deg

α_s blade mean-section stagger angle measured from axial direction, deg

β relative gas-flow angle measured from axial direction, deg

γ ratio of specific heats

δ boundary-layer displacement thickness, ft

δ^* boundary-layer displacement-thickness parameter, defined as $\frac{\delta_{tot}}{s \cos \beta_1}$

δ_f length from blade surface to edge of free-stream region between blade wakes measured perpendicular to blade surface, ft

δ_{te} trailing-edge-thickness parameter, $\frac{t}{s \cos \beta_1}$

η adiabatic efficiency

Θ_{cr} squared ratio of critical velocity at turbine inlet to critical velocity at NACA standard sea-level temperature, $(V_{cr,0}/V_{cr,sl})^2$

θ boundary-layer momentum thickness, ft

θ^* momentum-thickness parameter defined as $\frac{\theta_{tot}}{s \cos \beta_1}$

$\overline{\theta}_{tot}$ effective momentum thickness based on turbine over-all performance, ft (see ref. 4)

μ gas viscosity, lb/(ft)(sec)

ρ gas density, lb/cu ft

σ blade solidity at mean section, c/s

ψ_T coefficient of aerodynamic loading (see ref. 13)

Subscripts:

cr conditions at Mach number of 1.0

4061

[redacted]

fs	free stream, or that condition between blade wakes
h	hub
l	referring to any particular value of l
m	mean
min	minimum
opt	optimum
p	pressure surface
ref	reference or base value
s	suction surface
sl	NACA standard sea-level conditions
t	tip
tot	total of suction- and pressure-surface values
u	tangential
x	axial
0	station just upstream of blade leading edge
1	station just inside blade trailing edge
2	station downstream of trailing edge where circumferentially uniform conditions exist
2-D	two-dimensional, considering mean-section profile only
3-D	three-dimensional, considering blade surface and passage end-wall boundary layer

Superscripts:

'	total state
"	relative total state

[redacted]

APPENDIX B

A METHOD OF DETERMINING OPTIMUM SOLIDITY

In reference 13 a method is developed for predicting an optimum solidity for turbomachine blading. In this method a coefficient of aerodynamic loading ψ_T is defined by equation (14a) of reference 13, which rewritten in the symbols of this report is

$$\psi_T = \frac{2 \cos \beta_2 \sin(\beta_0 - \beta_2)}{\cos \beta_0} \frac{s}{c_x} \tag{B1}$$

(In checking the derivation of ψ_T, it was found that the reference showed an exponent of 2 for the term corresponding to $\cos \beta_2$ by mistake. In order that ψ_T will always be positive, let the sense of the relative gas-flow angles measured from the axial direction be such that the term $\sin(\beta_0 - \beta_2)$ is always positive.)

The basic assumption used herein and in the reference is that the optimum solidity based on axial chord length $\sigma_{x,opt}$ would be defined by a ψ_T of 0.8 for any set of inlet and outlet flow angles. Thus, $\sigma_{x,opt}$ can be obtained from the equation

$$\sigma_{x,opt} = \left(\frac{c_x}{s}\right)_{opt} = \frac{2.5 \cos \beta_2 \sin(\beta_0 - \beta_2)}{\cos \beta_0} \tag{B2}$$

In order to obtain the optimum solidity based on blade chord length σ instead of that based on the axial chord length σ_x from equation (B2), it is necessary to determine the stagger angle α_s (fig. 11), because the two solidity values are related as follows:

$$\sigma = \frac{\sigma_x}{\cos \alpha_s} \tag{B3}$$

The stagger angle α_s can be closely approximated by assuming that the blades are designed as shown in figure 11, with the assumptions that

(1) The leading and trailing edges have zero thickness.

(2) The suction-surface lengths from J to K and from L to M are straight and set at angles equal to the inlet and outlet flow angles, respectively.

(3) The suction surface from K to L is a circular arc of radius a. To simplify the development, let the blade spacing s be equal to 1.0; then, c_x is equal to σ_x, and some of the lengths shown in figure 11 can be expressed as trigonometric functions only. In the development, the inlet flow angle β_0 is considered positive, and the outlet flow angle β_2 is considered negative as shown.

From figure 11 it can be seen that

$$\sigma_x = \sin \beta_0 \cos \beta_0 + a \sin \beta_0 - a \sin \beta_2 - \sin \beta_2 \cos \beta_2 \tag{B4}$$

By rearranging equation (B4),

$$a = \frac{\sigma_x - \sin \beta_0 \cos \beta_0 + \sin \beta_2 \cos \beta_2}{\sin \beta_0 - \sin \beta_2} \tag{B5}$$

Substituting equation (B2) into equation (B5) gives

$$a = \frac{2.5 \cos \beta_2 \sin(\beta_0 - \beta_2) - \sin \beta_0 \cos^2 \beta_0 + \cos \beta_0 \sin \beta_2 \cos \beta_2}{\cos \beta_0 (\sin \beta_0 - \sin \beta_2)} \tag{B6}$$

The stagger angle is given by

$$\alpha_s = \tan^{-1} \frac{j}{\sigma_x} \tag{B7}$$

and, from figure 11,

$$j = \sin^2 \beta_0 - a(\cos \beta_0 - \cos \beta_2) - \sin^2 \beta_2 \tag{B8}$$

The value of the stagger angle is thus defined by the inlet and outlet flow angles β_0 and β_2, because a, j, and σ_x are functions of these two angles. Therefore, the value of the optimum solidity σ_{opt} can be determined by substituting the values of β_0 and β_2 into equations (B2), (B6), and (B8) and solving equation (B3).

For a range of inlet and outlet flow angles that usually occur in turbines, the optimum solidity was calculated. Figure 10 presents the results of these calculations, which were limited for the most part to reaction blading.

APPENDIX C

EFFECT OF VARYING TRAILING-EDGE BLOCKAGE

In addition to the viscous loss along the blade surface, there is a total-pressure loss resulting from the mass-flow void behind the blade trailing edge (fig. 1). Theoretical investigations of the effect of trailing-edge blockage on blade losses including mixing are reported in references 1 and 17, and an experimental investigation of the effect of a reduction in turbine stator trailing-edge thickness is reported in reference 12. Also, results of an investigation of the effect of trailing-edge thickness on the drag of an airfoil in the Mach number range of 0.7 to 1.6 are given in reference 18. In each of these references the losses including mixing increase with both trailing-edge thickness and Mach number.

Even though the magnitude of the change in total-pressure loss for a given change in trailing-edge blockage cannot be accurately determined from theory (see ref. 12), at least the trends of the total-pressure loss with variations in trailing-edge blockage can be approximated.

Variation of Trailing-Edge Thickness Only

For a variation in trailing-edge thickness only, the conditions inside the trailing edge (station 1 in fig. 2) can be approximated from specified design conditions at station 2. From the design weight-flow parameter at station 2, $\left(\frac{\rho W_x}{\rho'' W_{cr}}\right)_2$, the weight-flow parameter at station 1 can then be determined by considering the reduction in flow area attributed to trailing-edge blockage by

$$\left(\frac{\rho W_x}{\rho'' W_{cr}}\right)_1 = \left(\frac{\rho W_x}{\rho'' W_{cr}}\right)_2 \left(\frac{s}{s - \frac{t}{\cos \beta_2}}\right) \tag{C1}$$

The flow angle at station 2, β_2, is used in equation (C1) because it would be specified by the velocity diagram and it closely agrees with β_1 in most cases. Assuming no change in the whirl component of the velocity,

$$\left(\frac{W_u}{W_{cr}}\right)_1 = \left(\frac{W_u}{W_{cr}}\right)_2 \tag{C2}$$

Then by means of a "weight-flow" chart for the appropriate value of the ratio of specific heats γ, such as figure 3 of reference 19, the critical

velocity ratio at station 1, $\left(\frac{W}{W_{cr}}\right)_{fs,1}$, can be determined for the values obtained in equations (C1) and (C2). The value of β_1 can then be obtained from

$$\beta_1 = \sin^{-1}\left(\frac{W_u}{W}\right)_{fs,1} \tag{C3}$$

A small increase in t results in a comparatively small decrease in β_1. Then, assuming that θ_{tot} is constant during changes of t, the value of $\theta^*_{3\text{-}D}$ decreases with an increase in t because of the decrease in the value of β_1 (see eqs. (6) and (12)).

In the method of computing a loss total-pressure ratio given in reference 3, the displacement-thickness parameter $\delta^*_{3\text{-}D}$ is computed from the equation

$$\delta^*_{3\text{-}D} = H\theta^*_{3\text{-}D} \tag{C4}$$

where H is the form factor, and its values used herein correspond to a simple-power-law velocity profile with an exponent n of 1/7. The form factor H is a function of $\left(\frac{W}{W_{cr}}\right)_{fs,1}$, and increases as $\left(\frac{W}{W_{cr}}\right)_{fs,1}$ increases. Thus, H increases to some small degree with an increase in trailing-edge blockage. However, $\delta^*_{3\text{-}D}$ decreases only slightly with an increase in t, because the increase in H is counteracted by a slight decrease in $\theta^*_{3\text{-}D}$.

The trailing-edge-thickness parameter is defined as

$$\delta_{te} = \frac{t}{s \cos \beta_1} \tag{C5}$$

The value of δ_{te} is directly increased by an increase in t, and this increase is only slightly counteracted by the accompanying decrease in β_1.

Because the increase in t results directly in an increase in δ_{te} and indirectly in relatively small decreases in $\theta^*_{3\text{-}D}$ and $\delta^*_{3\text{-}D}$, the blade loss total-pressure ratio decreases with an increase in t as shown by figure 9 for any specified number of blades.

Variation of Number of Blades Only

Consider next a variation of the number of blades N only while maintaining constant solidity, trailing-edge thickness, blade height, and blade outlet velocity and angle at station 2. Such a change in N would vary the trailing-edge blockage and the blade spacing s. An increase in s would increase β_1 toward its limiting value β_2, and it would also decrease the value of b/s. A decrease in b/s could result in either an increase or decrease in θ^*_{3-D}, depending on the range of values of b/s, as can be seen by equation (12). With a change in θ^*_{3-D}, there would be a corresponding change in δ^*_{3-D} of equation (C4), affected only slightly by a small change in H with a small change in $\left(\frac{W}{W_{cr}}\right)_{fs,1}$. Also, an increase in s and the resulting small increase in β_1 would result in a decrease in δ_{te} of equation (C5).

The effect of the change in s (represented by a change in N in fig. 9) on the loss total-pressure ratio for a δ_{te} equal to zero is shown by the curve for t equal to 0 in figure 9. This curve of loss total-pressure ratio indicates the same trend as that for the momentum-thickness parameter shown in figure 7(a), considering the change in the shape of the curve as a result of using two different abscissas to represent the change in blade number N. The effect of varying the trailing-edge thickness t, which corresponds to changing δ_{te}, is shown for a range of values of t and N in figure 9, which is based on the stator of reference 8.

Trailing-Edge Blockage Considerations

As previously mentioned, the total-pressure loss increases as the trailing-edge thickness increases for a given number of blades; therefore, thin trailing edges are desirable from an aerodynamic standpoint. However, stress limitations and fabrication practices sometimes restrict the designer from specifying thin trailing edges. Even so, an attempt should be made to reduce the trailing-edge thickness as much as good judgment will allow.

Considering the fact that there must be a finite trailing-edge thickness, which results in a flow blockage at the trailing edge, an approximation of the optimum number of blades can be determined by calculating the loss total-pressure ratio p''_2/p''_0 over a range of values of t and N and plotting the results on a family of curves such as those

shown in figure 9. The point where p_2''/p_0'' is a maximum would be the best design configuration based on the theory.

Because the variation of blade loss with trailing-edge blockage depends on the outlet flow angle as well as the blade outlet Mach number (ref. 1), the effect of varying trailing-edge blockage will vary from design to design. Therefore, for each design, a series of loss total-pressure ratios would have to be calculated as previously discussed to determine the effect of deviating from an optimum trailing-edge blockage. For example, figure 9 presents such a variation in loss total-pressure ratio for the stator of reference 8 with a design outlet critical velocity ratio of 1.11 at a design angle of 62°. For this stator, it can be seen that for trailing-edge thicknesses on the order of 0.010 inch the effect of varying the number of blades is small, but for thicknesses on the order of 0.050 inch the effect of varying the number of blades is large. These loss trends for varying blockages are similar to those that would be obtained for any other blade configuration, except that for lower exit velocities the effect of blockage would not be as great (ref. 1).

The relative importance of trailing-edge thickness depends largely on the ranges of blockage and Mach number being considered and the effect on over-all performance (see ref. 12). A value of δ_{te} under 0.05 would not be considered detrimental in most cases, but values of δ_{te} over this value should be examined from the standpoint of the effect of blockage on the loss total-pressure ratio. It is possible, as indicated by figure 9, that high blockages could result in high losses in total pressure. Therefore, the selection of the final blade configuration should be guided to some extent by the contribution of the trailing-edge blockage to the over-all total-pressure loss.

REFERENCES

1. Stewart, Warner L.: Analysis of Two-Dimensional Compressible-Flow Loss Characteristics Downstream of Turbomachine Blade Rows in Terms of Basic Boundary-Layer Characteristics. NACA TN 3515, 1955.

2. Whitney, Warren J., Stewart, Warner L., and Miser, James W.: Experimental Investigation of Turbine Stator-Blade-Outlet Boundary-Layer Characteristics and a Comparison with Theoretical Results. NACA RM E55K24, 1956.

3. Stewart, Warner L., Whitney, Warren J., and Wong, Robert Y.: Use of Mean-Section Boundary-Layer Parameters in Predicting Three-Dimensional Turbine Stator Losses. NACA RM E55L12a, 1956.

4. Stewart, Warner L., Whitney, Warren J., and Miser, James W.: Use of Effective Momentum Thickness in Describing Turbine Rotor-Blade Losses. NACA RM E56B29, 1956.

5. Ainley, D. G., and Mathieson, G. C. R.: An Examination of the Flow and Pressure Losses in Blade Rows of Axial Flow Turbines. Rep. No. R.86, British N.G.T.E., Mar. 1951.

6. Schlichting, H.: Boundary Layer Theory. McGraw-Hill Book Co., Inc., 1955, pp. 430-447.

7. Miser, James W., Stewart, Warner L., and Monroe, Daniel E.: Effect of High Rotor Pressure-Surface Diffusion on Performance of a Transonic Turbine. NACA RM E55H29a, 1955.

8. Miser, James W., Stewart, Warner L., and Wong, Robert Y.: Effect of a Reduction in Stator Solidity on Performance of a Transonic Turbine. NACA RM E55L09a, 1956.

9. Heller, Jack A., Whitney, Rose L., and Cavicchi, Richard H.: Experimental Investigation of a Conservatively Designed Turbine at Four Rotor-Blade Solidities. NACA RM E52C17, 1952.

10. Hauser, Cavour H., and Nusbaum, William J.: Experimental Investigation of Effect of High-Aspect-Ratio Rotor Blades on Performance of Conservatively Designed Turbine. NACA RM E54C18, 1954.

11. Balje, O. E.: A Contribution to the Problem of Designing Radial Turbomachines. Trans. A.S.M.E., vol. 74, no. 4, May 1952, pp. 451-472.

12. Whitney, Warren J., Stewart, Warner L., and Wong, Robert Y.: Effect of Reduced Stator-Blade Trailing-Edge Thickness on Over-All Performance of a Transonic Turbine. NACA RM E55H17, 1955.

13. Zweifel, O.: Optimum Blade Pitch for Turbomachines with Special Reference to Blades of Great Curvature. The Eng. Digest, vol. 7, no. 11, Nov. 1946, pp. 358-360; cont., vol. 7, no. 12, Dec. 1946, pp. 381-383.

14. Chanes, Ernest R., and Carman, L. Robert: The Effect of Inlet Temperature and Pressure on the Efficiency of a Single-Stage Impulse Turbine with a 13.2-Inch Wheel Pitch-Line Diameter. NACA WR E-232, 1945. (Supersedes NACA ARR E5H10.)

15. Wislicenus, George F.: Fluid Mechanics of Turbomachinery. McGraw-Hill Book Co., Inc., 1947, pp. 54-70.

16. Davis, Hunt, Kottas, Harry, and Moody, A. M. G.: The Influence of Reynolds Number on the Performance of Turbomachinery. Trans. A.S.M.E., vol. 73, no. 5, July 1951, pp. 499-509.

17. Reemen, J., and Simonis, E. A.: The Effect of Trailing Edge Thickness on Blade Loss. Tech. Note No. 116, British R.A.E., Mar. 1943.

18. Morrow, John D.: Measurements of the Effect of Trailing-Edge Thickness on the Zero-Lift Drag of Thin Low-Aspect-Ratio Wings. NACA TN 3550, 1955. (Supersedes NACA RM L50F26.)

19. Alpert, Sumner, and Litrenta, Rose M.: Construction and Use of Charts in Design Studies of Gas Turbines. NACA TN 2402, 1951.

TABLE I. - DATA FOR FIVE EXAMPLE TURBINES

[Design values are based on conditions at blade mean radius.]

Number of blades, N	64	44	32	24	88
Solidity, σ	2.586	1.778	1.293	0.970	1.778
Aspect ratio, $\mathscr{A}$	1.97	1.97	1.97	1.97	3.94
Equivalent specific work output, $\Delta h'/\theta_{cr}$, Btu/lb	16.68	16.14	16.51	16.66	16.14
Adiabatic efficiency at design specific work output and speed, η	0.870	0.891	0.886	0.865	0.887
Trailing-edge thickness, t, in.	0.030	0.030	0.030	0.030	0.015
Rotor-outlet relative critical velocity ratio, $(W/W_{cr})_2$	0.833	0.854	0.892	0.935	0.854
Rotor-outlet relative flow angle, β_2, deg	49.9	48.1	45.6	43.0	48.1

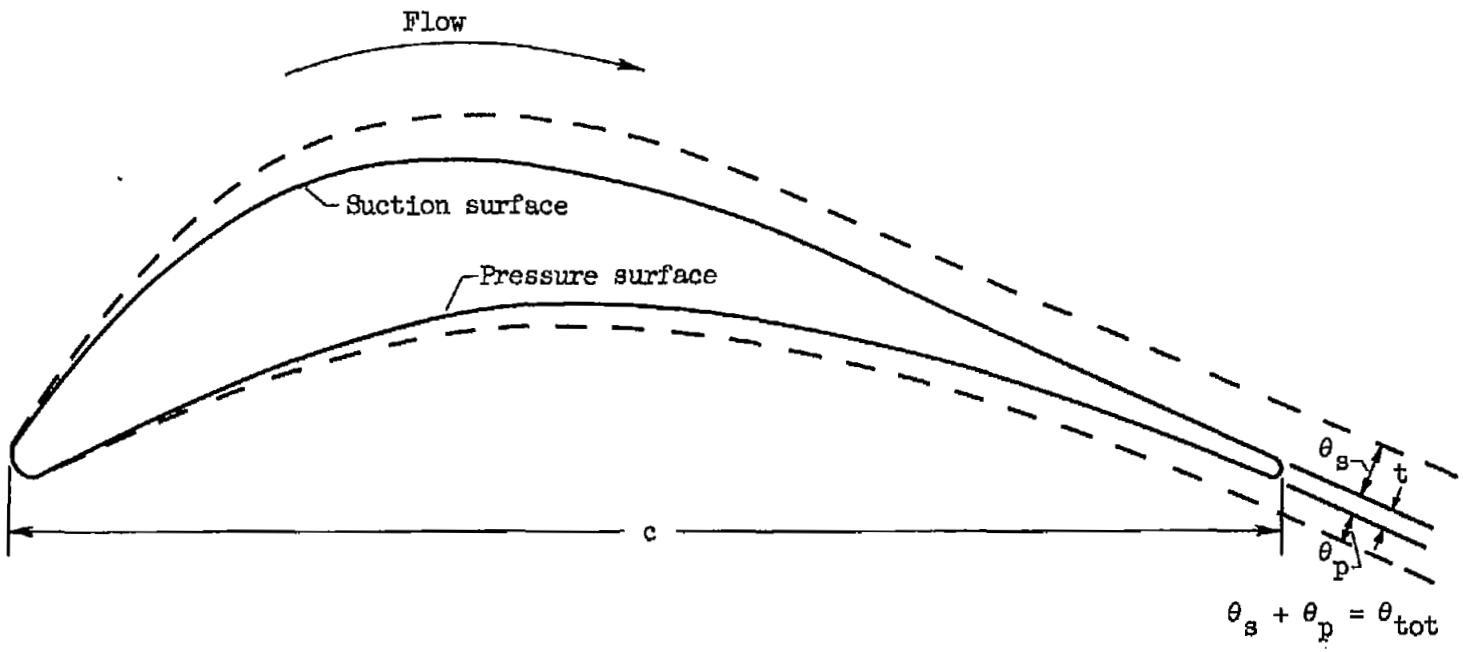

Figure 1. - Typical blade indicating momentum loss characteristics due to boundary layer and mass-flow void behind trailing edge.

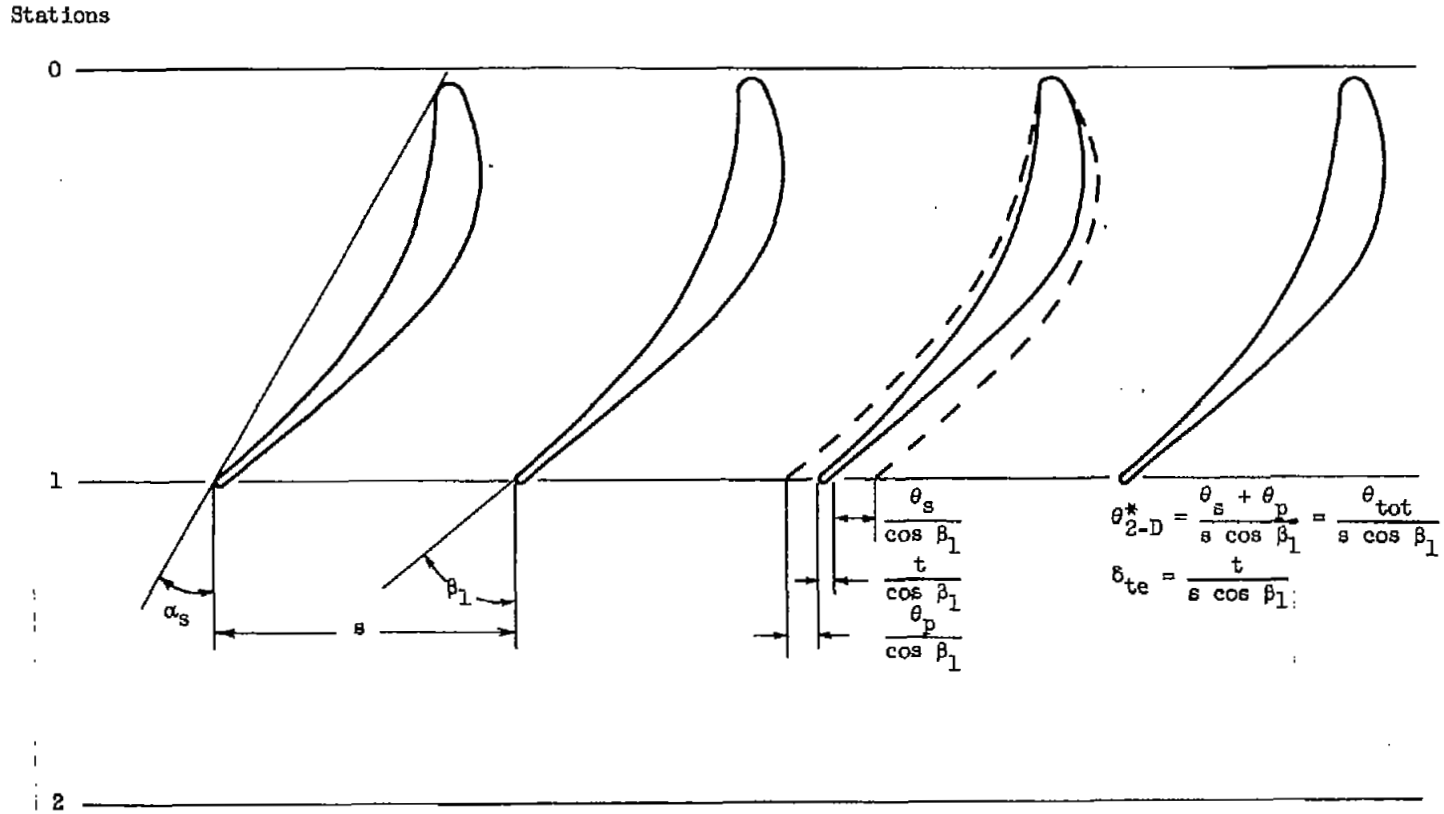

Figure 2. - Boundary-layer characteristics for two-dimensional cascade.

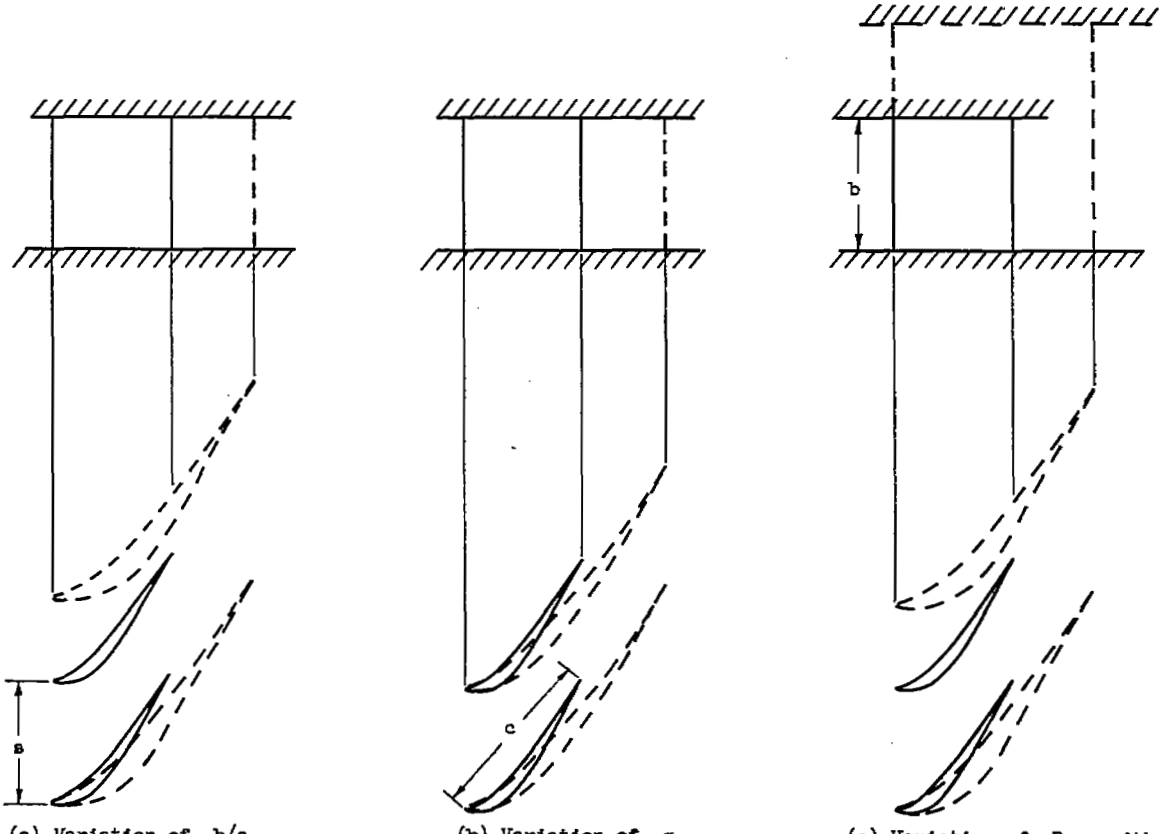

(a) Variation of b/s (σ and Re_b constant).

(b) Variation of σ (b/s and Re_b constant).

(c) Variation of Re_b with change in b only (b/s and σ constant).

Figure 3. - Variation of blade configuration with each of the three following independent variables: (a) blade height-to-spacing ratio b/s, (b) solidity σ, and (c) height Reynolds number Re_b.

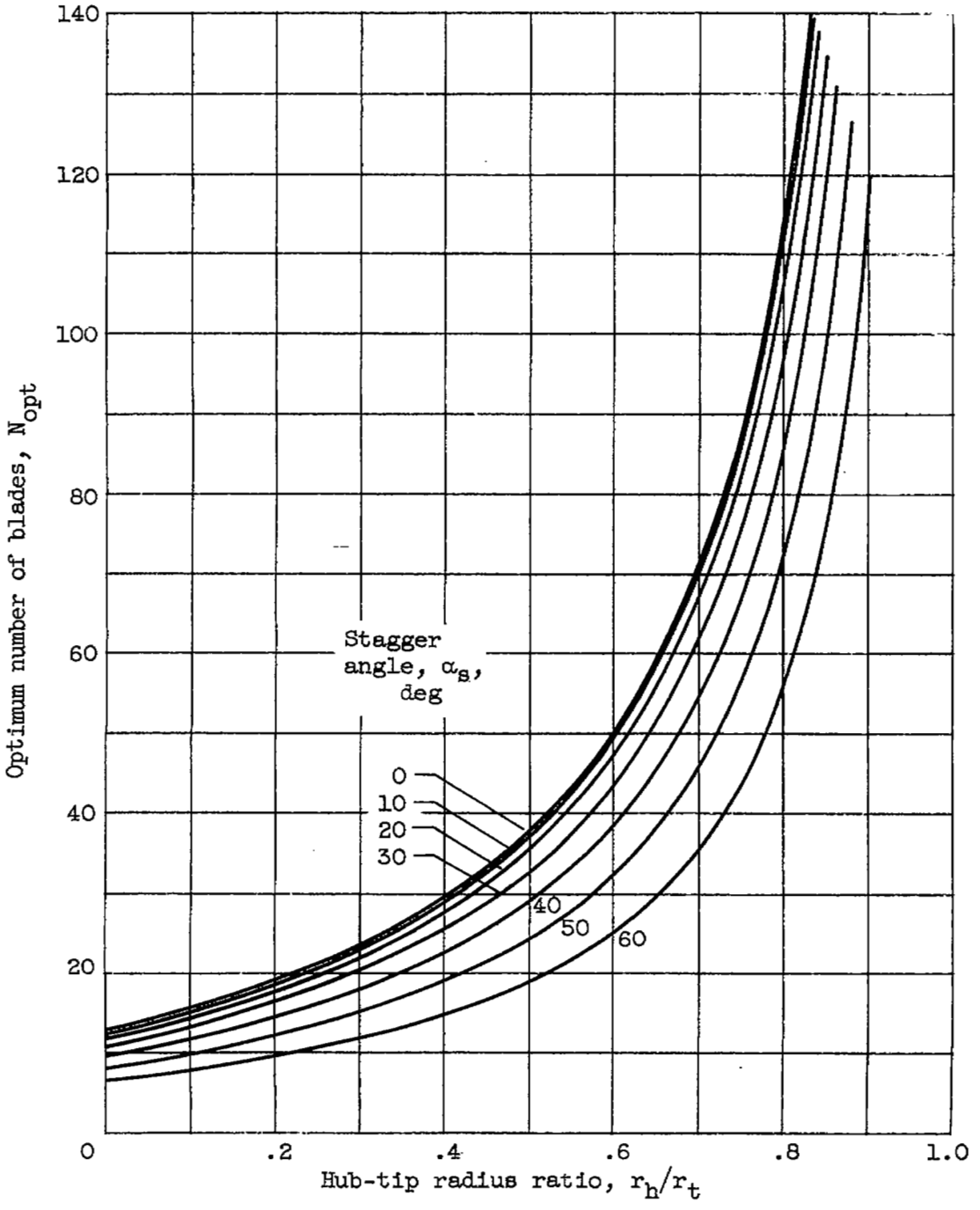

Figure 4. - Optimum number of blades for ranges of hub-tip ratio and stagger angle, considering only blade viscous loss. Exponent m, 1/5.

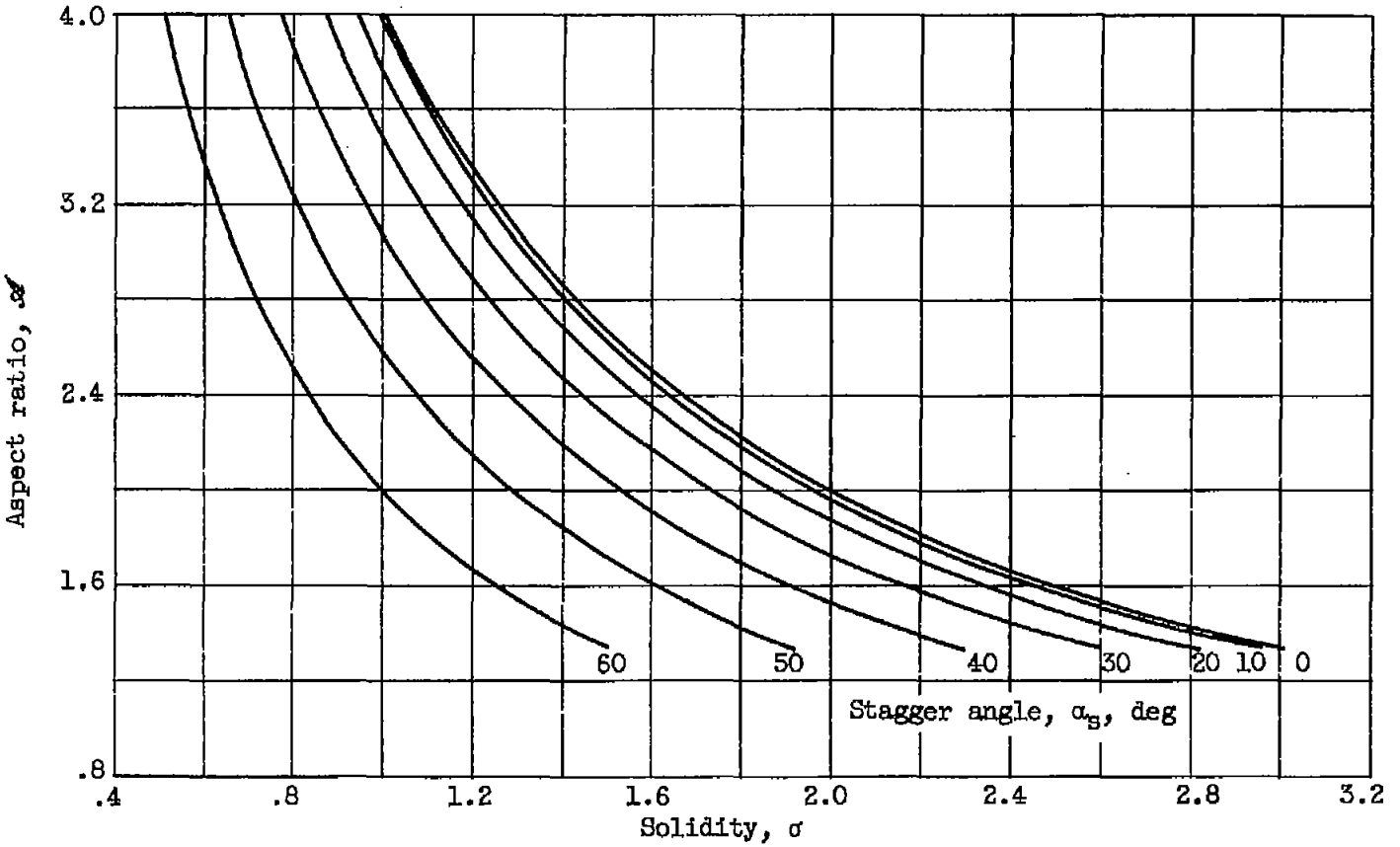

Figure 5. - Variation in aspect ratio corresponding to minimum viscous loss for a given solidity over range of stagger angles. Exponent m, 1/5.

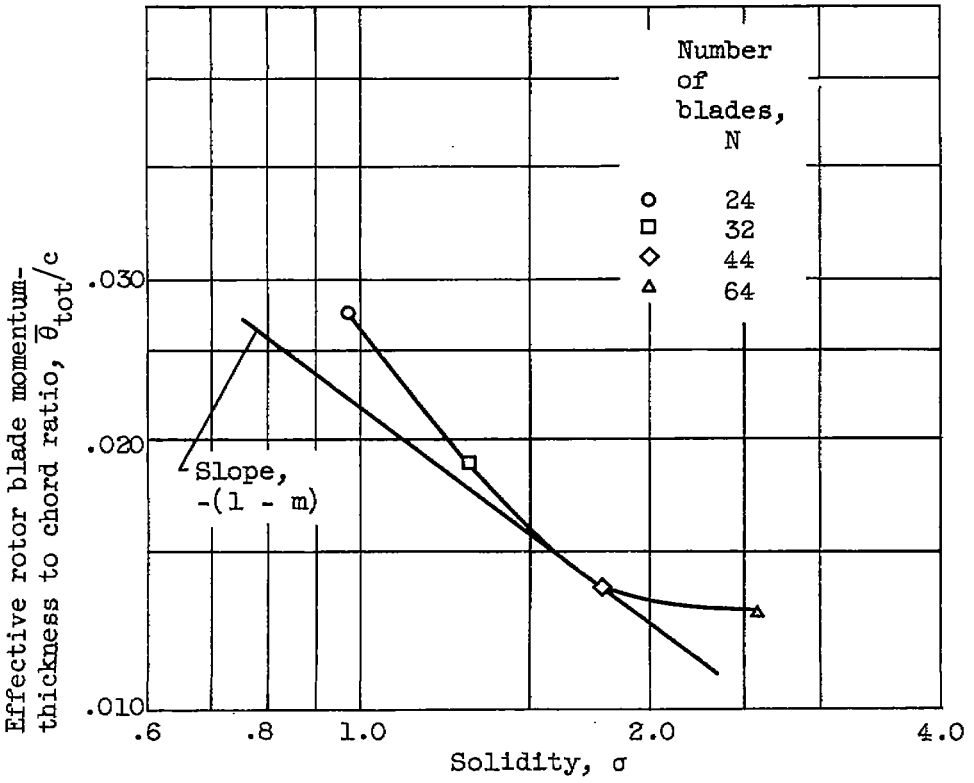

Figure 6. - Variation of effective rotor blade momentum-thickness to chord ratio with solidity based on results of four turbines of reference 9. Exponent m, 1/5.

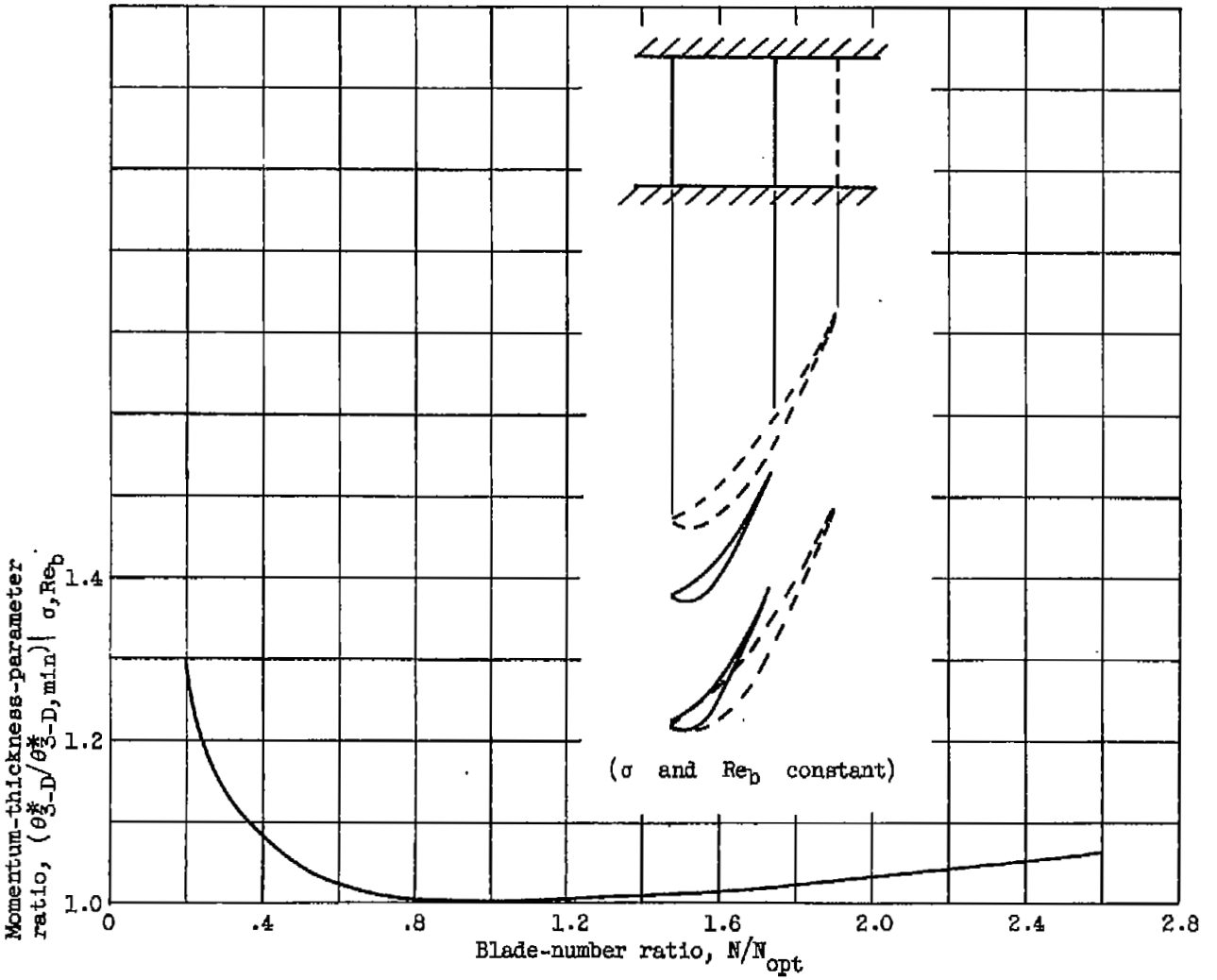

(a) Variation with blade-number ratio.

Figure 7. - Variation of momentum-thickness-parameter ratio. Exponent m, 1/5.

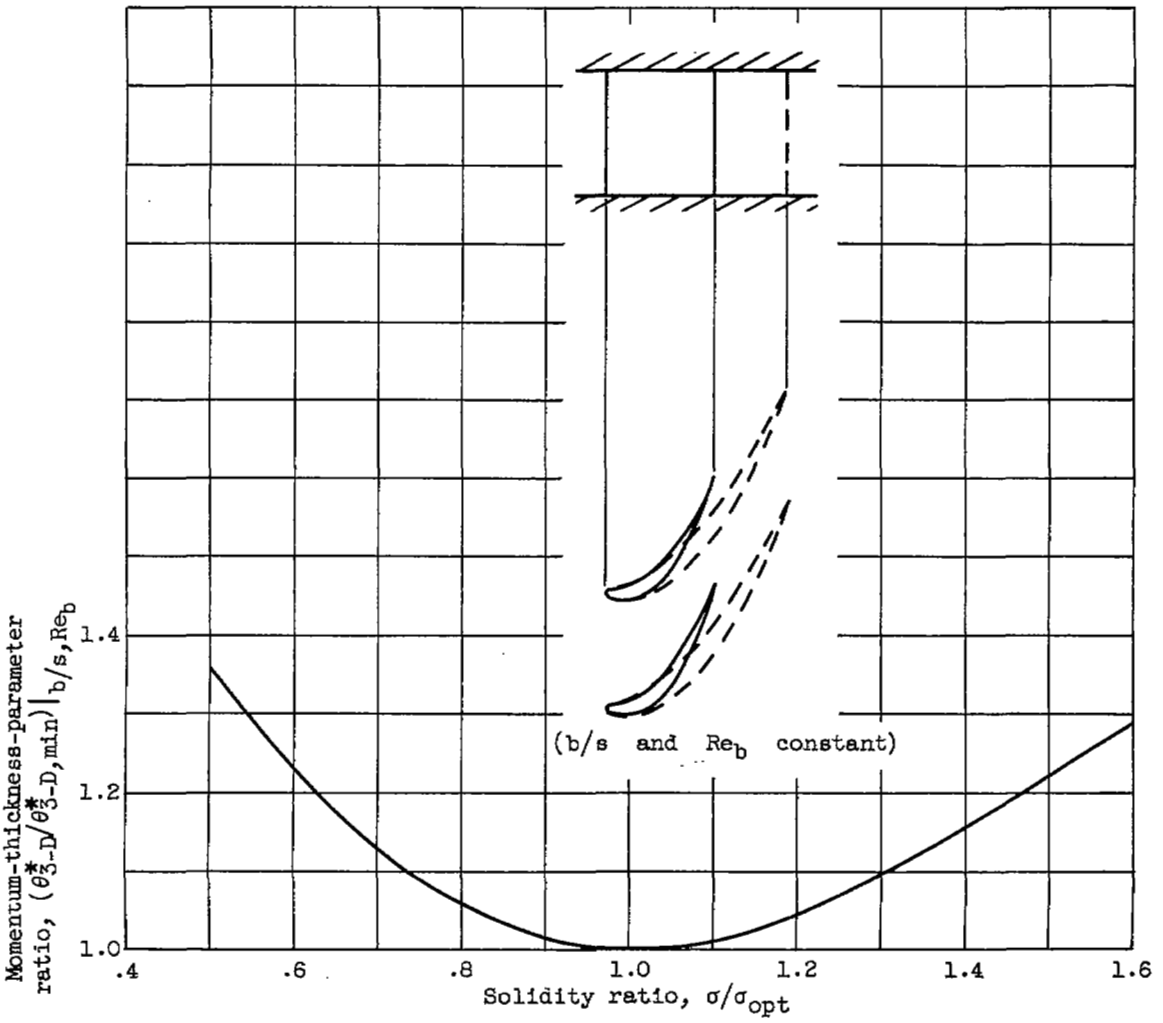

(b) Variation with solidity ratio.

Figure 7. - Continued. Variation of momentum-thickness-parameter ratio. Exponent—m, 1/5.

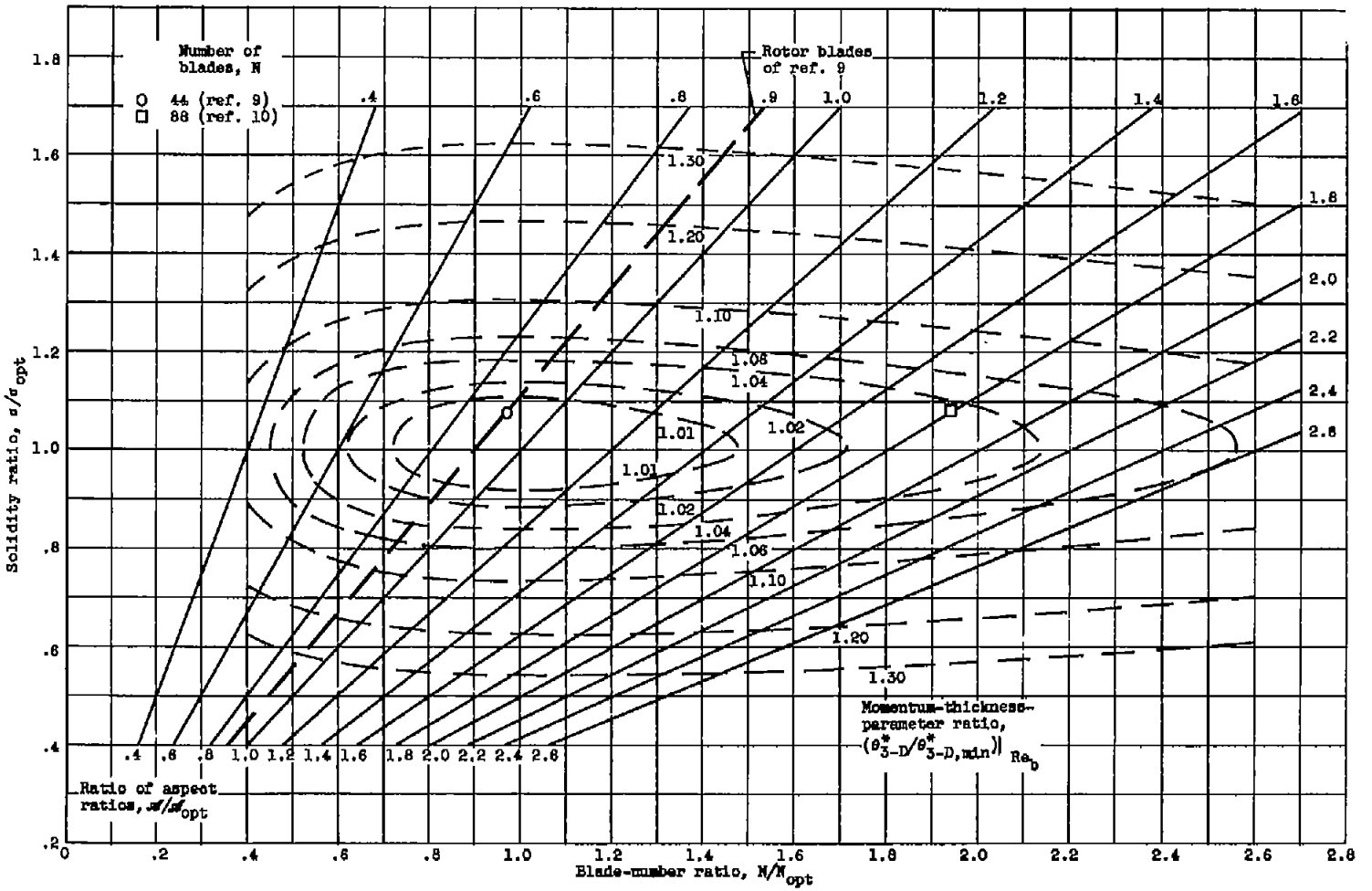

(c) Variation with solidity ratio, blade number, and ratio of aspect ratios for blades of constant height Reynolds number.

Figure 7. - Continued. Variation of momentum-thickness-parameter ratio. Exponent m, 1/3.

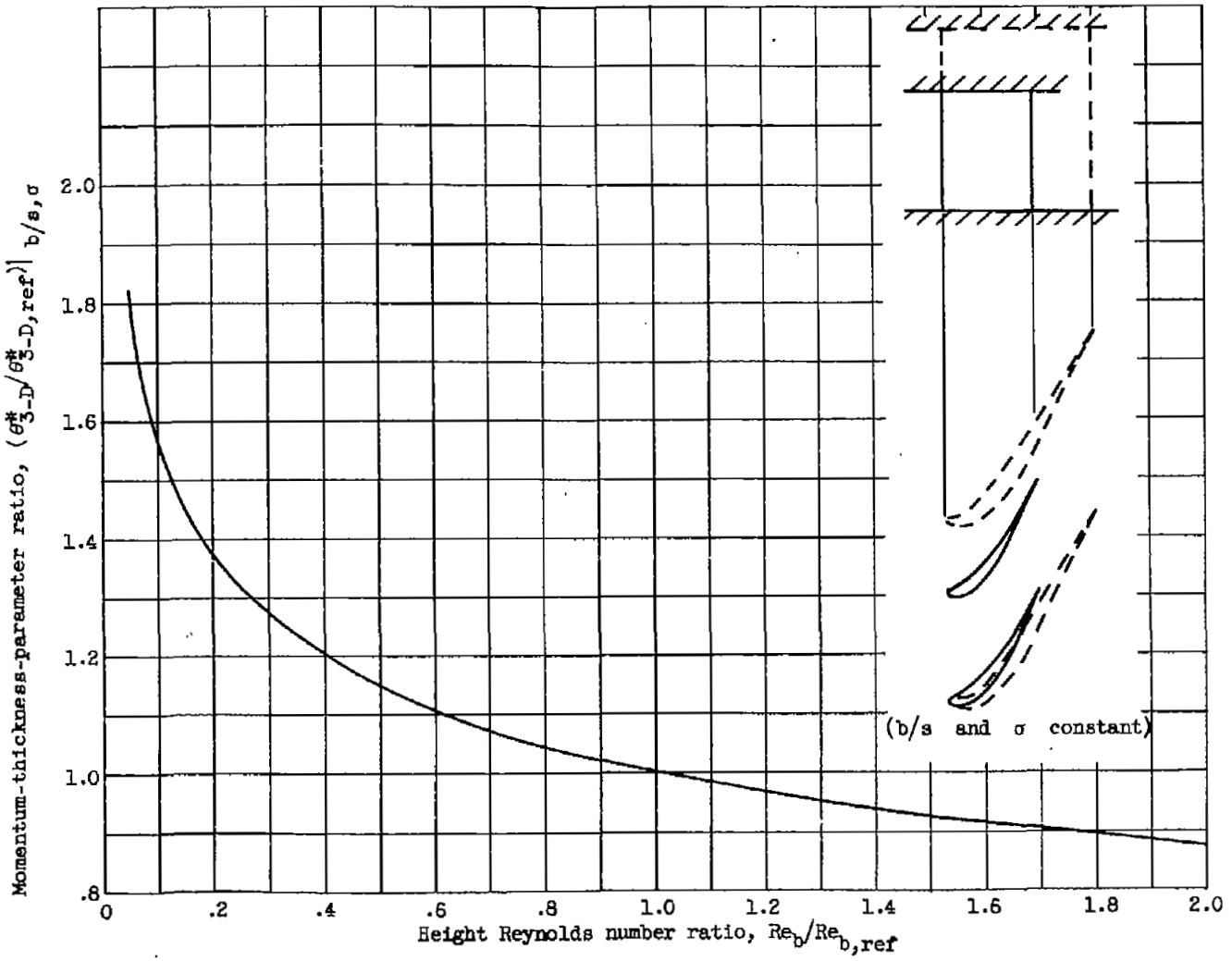

(d) Variation with height Reynolds number ratio.

Figure 7. - Concluded. Variation of momentum-thickness-parameter ratio. Exponent m, 1/5.

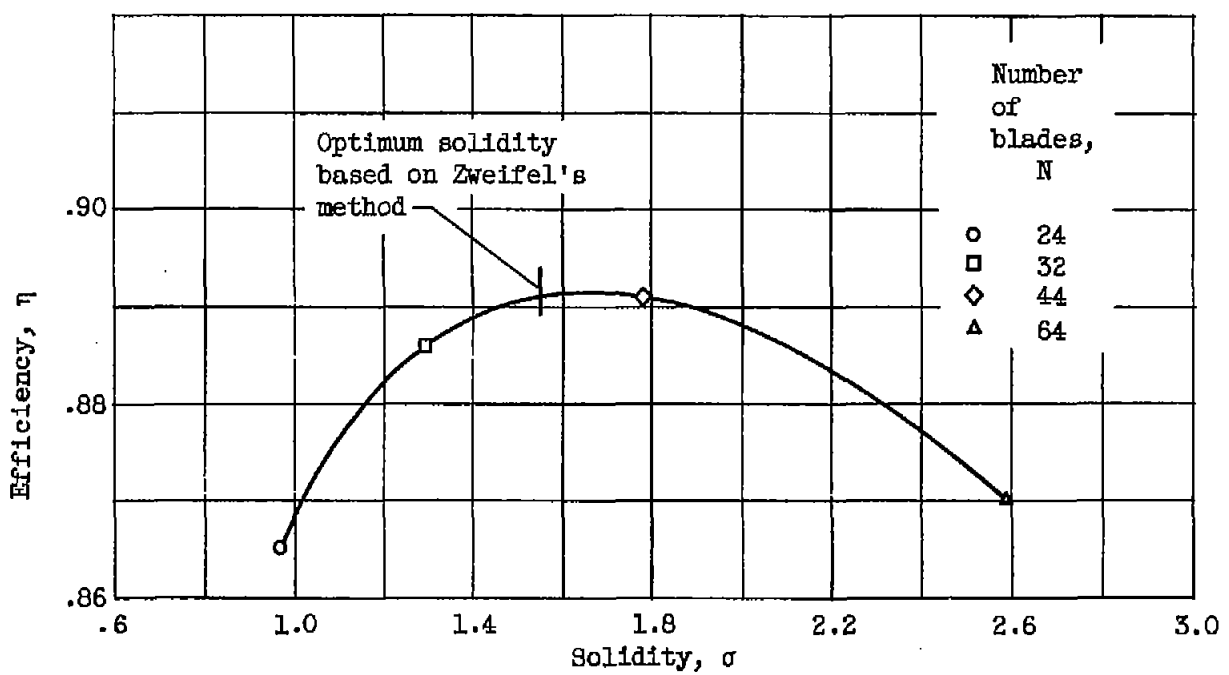

Figure 8. - Variation of efficiency with solidity for four turbines of reference 9.

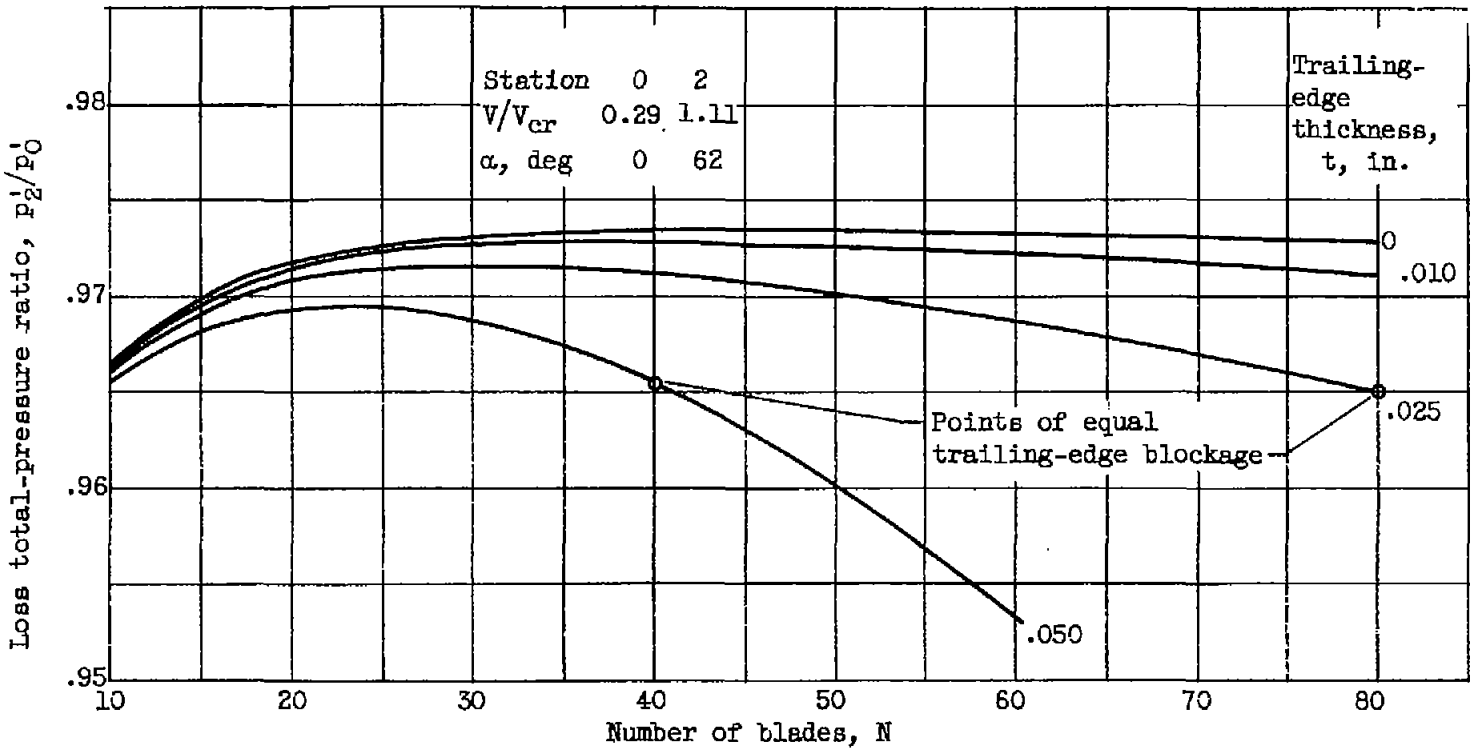

Figure 9. - Variation of loss total-pressure ratio with number of blades and trailing-edge thickness for stator of reference 12. Tip radius, 7.0 inches; hub-tip ratio, 0.7.

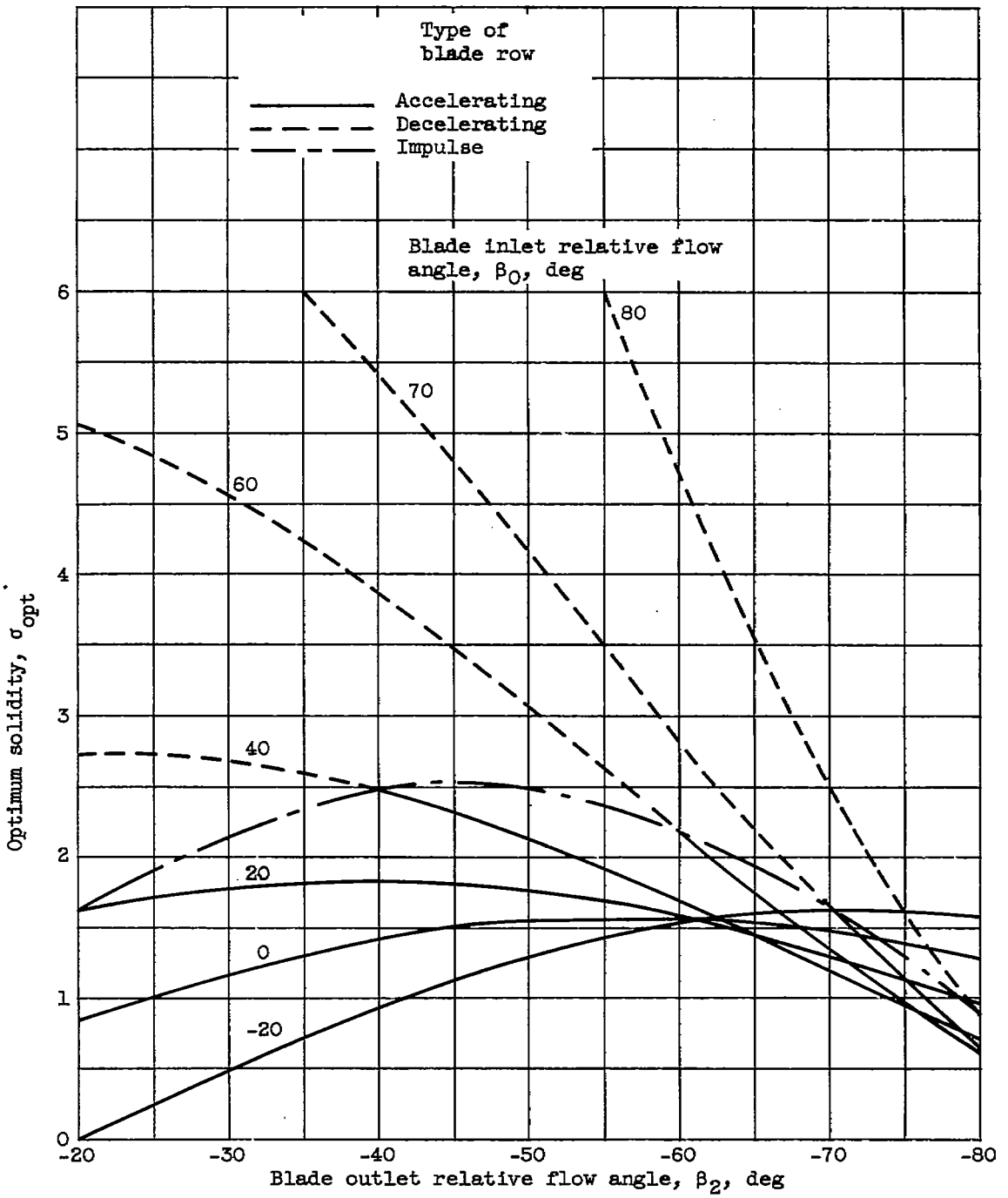

Figure 10. - Optimum solidity for a range of blade inlet and outlet relative flow angles, based on assumptions of reference 13.

[redacted]

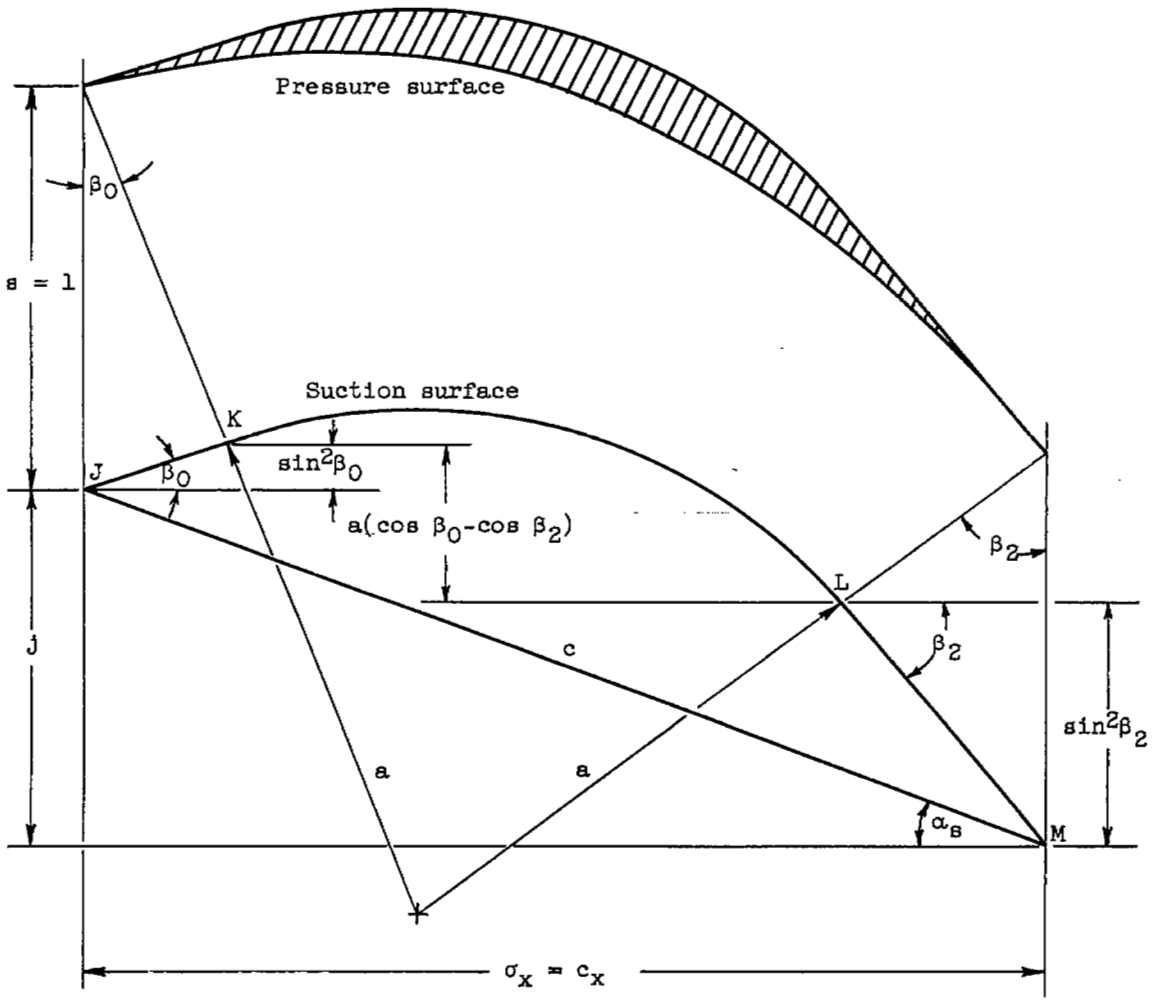

Figure 11. - Blade design variables used in determining stagger angle.